Research Article

The Journal of Comparative Neurology
Research in Systems Neuroscience
DOI 10.1002/cne.24317

Accepted Article

Title: Post-Mortem DTI Reveals Altered Hippocampal Connectivity in Wild Sea Lions Diagnosed with Chronic Toxicosis from Algal Exposure

Authors: Peter F. Cook,[1,2] Gregory S. Berns,[2] Kathleen Colegrove,[3] Shawn Johnson,[4] Frances Gulland[4]

Affiliations: 1. Long Marine Lab, University of California Santa Cruz, 95060, USA 2. Department of Psychology, Emory University, 30322, USA 3. College of Veterinary Medicine, University of Illinois at Urbana-Champaign, 60513, USA 4. The Marine Mammal Center, Sausalito, CA, 94965 USA

Abbreviated Title: Altered Hippocampal Connectivity in Wild Sea Lions

Requested Associate Editor: Oswald Steward

Key Words: Domoic Acid, Diffusion Tensor Imaging, Fornix, Sea Lions, Epilepsy

Corresponding author: Peter F. Cook, pcook930@gmail.com, 831-535-2686, New College Florida, Sarasota, FL 34234

This article has been accepted for publication and undergone full peer review but has not been through the copyediting, typesetting, pagination and proofreading process which may lead to differences between this version and the Version of Record. Please cite this article as an 'Accepted Article', doi: 10.1002/cne.24317
© 2017 Wiley Periodicals, Inc.
Received: Jun 13, 2017; Revised: Aug 16, 2017; Accepted: Aug 17, 2017

This article is protected by copyright. All rights reserved.

Accepted Article

Abstract

Hundreds of wild California sea lions (*Zalophus californianus*) exposed to the algal neurotoxin domoic acid are treated in veterinary rehabilitation centers each year. Common chronic effects of toxic exposure in these animals are seizures and hippocampal damage, and they have been proposed as a natural animal model for human epilepsy. Humans with medial temporal lobe epilepsy present with white matter pathology in a number of tracts including the fornix and increased structural connectivity between the hippocampus and thalamus. However, there are no prior data on structural connectivity in sea lion brains, with or without neuropathology. In the present study, we used a novel diffusion tensor imaging technique to obtain high resolution (1mm isotropic) white matter maps in brains obtained opportunistically post-mortem from wild sea lions with and without chronic clinical signs of toxic exposure to domoic acid. All animals had received a full veterinary workup and diagnosis prior to euthanasia. We measured hippocampal atrophy morphometrically, and all brains were examined histopathologically. In animals diagnosed with chronic domoic acid toxicosis, the fornix showed signs of altered diffusion properties indicative of pathology; these brains also had increased structural connectivity between hippocampus and thalamus in comparison to brains from animals with no neurological signs. These findings establish further parallels between human medial temporal lobe epilepsy and a naturally occurring condition in wild sea lions and simultaneously advance general knowledge of the deleterious effects of an increasingly common natural toxin.

Introduction

This article is protected by copyright. All rights reserved.

Accepted Article

Each year along the West coast, hundreds of sea lions are exposed in the wild to algal neurotoxin domoic acid (DA), come to shore in distress (i.e., strand), and are taken to veterinary rehabilitation facilities (Scholin et al., 2000; Goldstein et al., 2008). DA, the cause of "amnesic shellfish poisoning" in humans (Perl et al., 1990), binds preferentially to α-amino-3-hydroxy-5-methyl-4-isoxazolepropionic acid (AMPA) and kainate receptors (Silvagni et al., 2005), which are plentiful in mammalian hippocampus (Bernabeu and Sharp, 2000). Affected sea lions have been extensively studied in veterinary rehabilitation settings. Acute exposure in sea lions leads to excitotoxic cell death in the dentate gyrus and CA3 portion of the hippocampus (Pullido, 2008), and can cause seizures and death. Sea lions who survive initial exposure may develop chronic epilepsy and resultant hippocampal atrophy (Goldstein et al., 2008, Montie et al., 2010). They have also been shown to have potentially maladaptive spatial memory deficits and behavioral perseveration (Cook et al., 2011; Cook et al., 2015; Cook et al. 2016), disrupted navigation (Thomas et al., 2010), increased likelihood of restranding after release, and, in most cases, eventual mortality (Gulland et al., 2002). This chronic condition is recognized as a differentiable clinical diagnosis in wild sea lions with clear behavioral and pathophysiological correlates (Goldstein et al. 2008).

Both DA and kainic acid are used to produce laboratory models of seizure disorders (Lothman and Collins, 1981; Dakshinamurti et al., 1991), and the chronic effects of naturally occurring DA exposure in sea lions have been suggested to be largely analogous to medial temporal lobe (MTL) epilepsy in humans (Muha and Ramsdell, 2011; Ramsdell and Gulland, 2014). Like humans with MTL epilepsy, sea lions with DA toxicosis show cell death and mossy fiber sprouting in the dentate gyrus, and typically unilateral patterns of gross hippocampal atrophy. Due to these similarities, wild sea lions exposed to DA have been proposed as an accessible and

This article is protected by copyright. All rights reserved.

ecologically valid alternative medical model for human epilepsy (Buckmaster et al., 2014; Grone and Baraban, 2015). However, further study is needed to chart the extent of neurobiological effects of toxic exposure in wild sea lions, both for the sake of improving clinical treatment and assessing the validity of sea lions as a comparative model for disease.

In diffusion tensor imaging (DTI) studies, humans with MTL epilepsy show distributed white matter pathology, typically presenting as decreased fractional anisotropy (FA) and, in certain cases, increased mean diffusivity (MD), in a number of limbic pathways. Meta-analyses suggest damage is most pronounced in limbic tracts and those passing through the temporal lobe, including the fornix, cingulate, arcuate fasciculus, and uncinate fasciculus (Gross et al., 2011; Mishra et al., 2011; Otte et al. 2012; Govindan et al. 2008). Joint imaging and histology work in humans have linked decreased FA with decreased fiber bundle circumference and reduced myelination (Werring et al., 2000; Pierpaoli et al., 2001; Concha et al., 2010; Cruces & Concha, 2015). MTL epilepsy has also been shown to increase hippocampal structural connectivity (Bonilha et al., 2012), notably between the hippocampus and thalamus (Dinkelacker et al., 2015). There are no studies of structural connectivity in sea lions, but there is evidence of disrupted functional connectivity between the hippocampus and thalamus in wild sea lions with DA toxicosis (Cook et al., 2015), which matches findings of disrupted functional connectivity in humans with epilepsy (Waites et al., 2006; Liao et al., 2010) and rodents (Dugladze et al. 2007; Hiolski et al. 2016) and could be consistent with white matter reorganization and fornix pathology specifically.

Examination of white matter changes in wild sea lions with DA toxicosis may inform and support their potential use as a medical model. In addition, it may broaden understanding of the effects of natural exposure to DA. DA-producing algal blooms are increasingly prevalent, due in

This article is protected by copyright. All rights reserved.

Accepted Article

Accepted Article

large part to anthropogenic influence on the oceans (Anderson et al., 2008; Silver et al., 2010). Although sea lions are the most visible victims of DA poisoning, many other species are affected, potentially including humans (Lefebvre and Robertson, 2010; Lefebvre et al., 2016). More broadly, there have been no DTI studies of structural brain connectivity in aquatic carnivores—such studies may illuminate neurobiological adaptations to these animals' unique ecology.

Here, using a novel technique for obtaining high resolution DTI data in fixed brains (Miller et al., 2012; Berns et al., 2015), we acquired 1 mm isotropic diffusion data in 8 brains collected opportunistically from wild sea lions who were euthanized due to poor medical prognosis in a rehabilitation setting: four brains with gross signs of hippocampal atrophy and four without. Fractional anisotropy (FA) and mean diffusivity (MD), potential markers of white matter pathology, were measured in the fornix, which could be clearly and reliably demarcated in these subjects, and diffusion values in the pyramidal tract were used as a control tracts to assess non-specific baseline differences in white matter diffusivity across subjects. The total number of streamlines tracking between hippocampus and thalamus was also measured. These values were compared between DA brains and brains from animals with no neurological signs as determined by veterinary diagnosis informed by clinical examination, histopathology and hippocampal morphometrics.

Materials and Methods

Subjects

John Wiley & Sons

This article is protected by copyright. All rights reserved.

Accepted Article

Brains for this study were obtained opportunistically from animals euthanized for medical cause at The Marine Mammal Center in Sausalito, CA. Eight brains were imaged for DTI analysis, four brains showing gross signs of hippocampal atrophy during preliminary MRI scanning, and four with no evident signs of gross neuropathology. Brains had been extracted within 24 hours of animal death, and fixed in 10% formalin for two weeks at ~4.5 degrees C before being shipped to Emory University for diffusion imaging.

Final diagnoses used to group the brains for comparison were determined post-hoc by an experienced veterinarian drawing on all available information on each animal from admission to post-mortem examination (as in Cook et al. 2015), and in keeping with best clinical practice informed by over two decades of extensive veterinary research with this population (Scholin et al. 2000; Gulland et al. 2002; Goldstein et al. 2008; Kirkley et al. 2014). Sea lions were diagnosed with carcinoma, malnutrition, and domoic acid toxicosis as described in Grieg et al. (2005). Clinical diagnosis of DA toxicosis is based on the combination of clinical signs, elevated eosinophils on CBC, ultrasound evidence of cardiomyopathy, and histology. Most DA cases display neurologic signs of seizures, ataxia, head weaving, tremoring, central blindness, blepharospasm, coma, and abnormal behavior (Gulland et al., 2002, Goldstein et al., 2008, Zabka and Gulland, 2012). Chronic cases and those with cardiomyopathy are also lethargic and malnourished. Diagnoses were supported in all cases by histopathological examination of each brain (as in Silvagni et al., 2005; Goldstein et al., 2008).

Histopathology

Following imaging, brains were sectioned to include both sides of the hippocampus, and tissue sections were routinely embedded in paraffin, processed, and stained with hematoxylin and eosin

This article is protected by copyright. All rights reserved.

Accepted Article

for histopathologic evaluation. Specific neuropathology of domoic acid exposure in sea lions has been well established in prior histological work (Silvagni et al. 2005; Goldstein et al., 2008; Lefebvre et al. 2010; Buckmaster et al. 2014). Routine hematoxylin and eosin stains were chosen in the current study to efficiently highlight established neuropathology consistent with DA toxicosis if present, and also to screen broadly for other pathologic lesions.

Imaging

All imaging and imaging analysis was conducted by an individual blind to diagnoses. For imaging, the specimens were set in 2% agarose (Phenix Research Products Low EEO Molecular Biology Grade Agarose) combined with an insoluble mixture of 2 mM gadolinium (III) oxide (Acros Organics, Fisher Scientific) (Gutman et al., 2012; Berns et al., 2015). This both holds the sample in place during scanning and provides a low-intensity background to the brain tissue for visualization as well as mitigating susceptibility artifacts at the surface of the brain.

Imaging for this study was performed on a 3 T Siemens Trio scanner with standard gradients and a 32-channel head receive coil and used a similar protocol to that detailed in Berns et al. (2015). Post-mortem tissues have shorter T1 and T2 relaxation times in comparison to live tissue, which can reduce signal quality (Miller et al., 2012). Therefore, we used a diffusion-weighted steady-state free precession (DW-SSFP) sequence optimized to increase signal to noise ratio in dead brain tissue (Miller et al., 2012). One set of DW-SSFP images, weighted along 52 directions, was acquired for each brain (FOV = 128 mm, voxel size = 1 mm isotropic, TR = 31 ms, TE = 24 ms, flip angle = 35°, bandwidth = 159 Hz/pixel, q = 255 cm^{-1}, G_{max} = 38.0 mT/m, gradient duration = 15.76 ms). Another five images were acquired for each brain with the same parameters except with q = 10 cm^{-1} applied in one direction only (these take the place of b=0 scans in conventional

This article is protected by copyright. All rights reserved.

spin-echo DTI acquisitions). An accurate model of the DW-SSFP signal for post-mortem tissue must include T1 and T2 values, which we calculated for each brain using T1-weighted images (TIR sequence with TR = 1000 ms, TE = 12 ms, and TI = 30, 120, 900 ms) and T2-weighted images (TSE sequence with TR = 1000 ms, TE = 14, 29, 43 ms). High-resolution (0.6 x 0.6 x 0.5 mm) structural reference images were acquired using a "trufi" 3D balanced SSFP sequence (TR = 7.09 ms, TE = 3.55 ms, flip angle = 37°). Balanced trufi images were acquired in pairs with the RF phase incrementing 0° and 180°, and were then averaged to reduce banding artifacts (Miller et al. 2011). Total acquisition for all scan sequences was approximately 7 hours for each brain. Mean B0 and trufi structural images were computed using FSL's fslmaths. Transforms were computed between diffusion and high-resolution structural space by affine transformation of the mean B0 image to the mean trufi image with FSL's FLIRT. The resultant transformation matrix was used to compute transformations from diffusion to high-resolution structural space and vice versa, for tracking and visualization respectively. All diffusion images were processed with modified FSL tools that account for the DW-SSFP signal model and incorporate T1 and T2 measures.

Tractography

Tractography was conducted with a modified version of BEDPOSTX that incorporated the new signal model (Buxton, 1993; McNab et al., 2009; Miller et al., 2011) with 2 crossing fibres per voxel (Behrens et al., 2007). For voxel-wise estimates of diffusion parameters, we used a similarly modified version of DTIFIT.

Probabilistic tract tracings were used to define the fornix and the pyramidal tract for comparison of diffusion parameters between groups. The pyramidal tract was used for control, as it does not

John Wiley & Sons

This article is protected by copyright. All rights reserved.

Accepted Article

typically show extensive pathology in MTL epilepsy. The number of streamlines tracking between right and left hippocampus and bilateral thalamus was also computed using probabilistic tract tracings and compared between groups. All tracts used in quantitative analysis were computed using hand-drawn anatomical ROIs as seeds and targets in PROBTRACKX from FSL's FDT toolkit (Behrens et al., 2003; Behrens et al., 2007). For all tracings, we used the default 5000 streamlines from each voxel, a step length of 0.5 mm, distance correction, and a standard curvature threshold of 80°.

For subsequent tract definition, probabilistic tracts were thresholded by voxel using percentage of total streamlines from seed to that voxel. There is no way to determine appropriate threshold *a priori*, so we used thresholds of 5%, 10%, and 20%, computing diffusion values at each threshold with appropriate statistical correction for multiple comparisons.

ROI and Seed definition

All probabilistic tracing for this study was conducted using hand-drawn anatomical seeds, in FSL's FSLview, consistent with anatomical designations established in a prior California sea lion brain atlas (Montie et al., 2009).

Fornix tract: To accurately trace the fornix without over-representing adjacent tracts, left and right fornix were traced separately for each brain using hand-placed 12-voxel seeds in the crus of the fornix. These seeds were drawn on the FA images in DTI space, in which the forniceal white matter was easiest to visualize. Seeds were drawn with an overlaid principal diffusion map on two adjacent slices in the transverse plane. Seeds were placed in white matter with clear rostro-caudal diffusion directionality, ventral to the corpus callosum and dorsal to the dorsal boundary of the thalamus. The rostral boundary of the seeds was just caudal to the ventral turn of the

This article is protected by copyright. All rights reserved.

Accepted Article

rostral fornix, well caudal to the caudal boundary of the septum pellucidim. Medial boundaries of the seeds were lateral to midline so that they did not overlap. Two termination masks were used in tracing—a planar mask in the transverse plane at the level of the ventral boundary of the splenium and a planar mask in the coronal plane at the level of the caudal boundary of the septum pellucidum. These exclusion masks terminated any tracts that may have traveled into the corpus callosum or the septum pellucidum respectively. In all cases, probabilistic tracts from these seeds were assessed at multiple thresholds for anatomical plausibility.

Pyramidal tract: Right and left pyramidal tracts were traced for each animal using hand-placed seeds drawn on the high resolution trufi images, in which the pyramidal tract was most easily delineated from surrounding brain-stem tissue. Seeds were drawn with overlaid principle diffusion map on two consecutive slices in the coronal plane. They were placed over the full extent of the cross-section of the pyramidal tract in the brain stem, with clear rostro-caudal directionality, just caudal to the caudal boundary of the pons. Seeds were transformed into DTI space when used in BEDPOSTX. Again, probabilistic tracts from these seeds were assessed at multiple thresholds for anatomical plausibility.

Hippocampal ROI: Left and right hippocampus were traced separately by an individual with expertise in sea lion medial temporal neuroanatomy. Images were traced in the transverse plane on the high resolution trufis, in which the lateral and medial boundaries of the hippocampus were most clear (Fig. 1). Anatomical criteria were similar to those used in Cook et al. (2015). Briefly, cornu ammonis (CA), dentate gyrus, alveus, and part of the subiculum were traced in the transverse plane following the long axis of the hippocampus. Because there are no clear criteria for delineating subiculum from CA in sea lion hippocampus, tissue was taken above the interpolated line connecting the medial-most portion of parahippocampal white matter and the

This article is protected by copyright. All rights reserved.

Accepted Article

medial-most point on the curve of the subiculum. Hippocampus was traced from just ventral to the ventral boundary of the splenium to the rostroventral boundary of the head of the hippocampus, adjacent to the interpeduncular fossa. Lateral and medial boundaries were primarily defined by the fluid filled structures surrounding the hippocampus.

Thalamic ROI: The whole bilateral thalamus was also traced in the transverse plane, from its dorsal to ventral boundary. Thalamus was traced on B0 images in DTI space, in which thalamic boundaries with surrounding gray matter were most clearly delineated (Fig. 1).

As mentioned, all tract-based quantitative measures in the current study were computed using probabilistic tracings from FSLs BEDPOSTX. However, fornix tracts were also visualized in DSI Studio (Yeh et al., 2013), which relies on an algorithm that estimates the orientation distribution functions (ODFs) by filtering out "noisy" fibers based on a quantitative anisotropy (QA) metric, representative of diffusion strength and analogous to FA. Whole-brain and fornix renderings were computed using these parameters (unless otherwise specified): QA threshold = 0.11, angular threshold = 55°, step size = 0.50 mm, minimum length = 20 mm. 3D images of tracts were also rendered at 5° increments of rotation of the brain and assembled into movies (Mov. 1 and 2).

Quantitative Analysis

To quantify gross changes to hippocampal volume, as typically seen in sea lions with chronic DA toxicosis (Goldstein et al., 2008), volumes of right and left hippocampus were computed as percentage of whole brain volume from the same masks used as seeds for hippocampal-thalamic connectivity as in Cook et al. 2015. Standard deviation and mean relative volume of the right and left hippocampus were then computed. Animals with either right or left hippocampus volume

This article is protected by copyright. All rights reserved.

more than one standard deviation below the sample mean (computed from all eight brains) were considered to have hippocampal atrophy.

Results of DTI tractography are somewhat variable based on subjectively assigned parameters, including thresholding of results (Thomas et al., 2014). However, tractography results have been repeatedly validated through both anatomical and functional connectivity approaches, and DTI is effective at capturing major fiber tracts (Catani et al., 2003; Guye et al., 2003; Wakana et al., 2004).

In the current study, fornix and pyramidal tracts were thresholded at 5%, 10%, and 20% of streamlines by voxel, then binarized. Binarized tracts at each threshold were used as masks to extract mean FA and MD values for each tract from the diffusion data maps.

For each subject, total number of streamlines tracking between right and left hippocampal seeds and bilateral thalamic endpoint was also computed. These numbers were corrected for size of hippocampal and thalamic masks so that animals with larger brain structures would not have artificially enhanced number of streamlines relative to smaller-brained subjects. Total number of streamlines for right and left hippocampus were divided by number of voxels in right and left hippocampal masks respectively, and then these values were divided by number of voxels in the bilateral thalamic masks.

Due to the small sample size in this study, standard inferential approaches may not be justified. Therefore, in addition to the qualitative observations, we used a Bayesian approach, employing Markov Chain Monte Carlo simulation (Zhao et al. 2006) to estimate the likelihood of achieving observed FA and MD values in both the control (pyramidal) and experimental (fornix) tracts between control and DA brains. Separate analyses were conducted with values from each

John Wiley & Sons

This article is protected by copyright. All rights reserved.

Accepted Article

Accepted Article

streamline threshold, 5%, 10%, and 20%. We also conducted a simulation based on number of corrected streamlines between hippocampus and thalamus in healthy and DA brains. These likelihoods were then used to compute Bayes Factors, representing the likelihood ratio of two contrasting hypotheses: 1) diffusion values differ between DA and control brains, over 2) diffusion values do not differ between DA and control brains. Analysis was conducted with the anovaBF function in the BayesFactor package (Morey, Rouder & Jamil, 2015) in the R statistical software package. This function accommodates repeated measures designs (Rouder et al. 2012), taking into account the presence of a right hemisphere and left hemisphere value for each animal for each tract in the present study. For each analysis, 10,000 simulations were carried out, allowing for convergence and explicit assessment of Bayes Factors. Bayes Factors were interpreted as in Lee and Wagenmakers (2013).

Results

General Features of Sea Lion White Matter Connectivity

In examining whole-brain, deterministic maps of white matter connectivity in control sea lions (Mov. 1), a number of features stand out. Cortical projections are highly inter-digitated in all hemispheres. However, there appears to be somewhat limited rostrocaudal cortical connectivity, with a clear directional division between rostrally projecting fibers rostral to the temporal sulcus, and caudally projecting fibers caudal to the temporal sulcus, as well as very sparse cingulate fibers. In addition, sea lion corpus callosum appears thin, suggesting limited interhemispheric connectivity. Olfactory pathways also appear very small in comparison to terrestrial carnivores. The fornix appears very similar to that observed in other mammals (Fig. 2). The pyramidal tract

John Wiley & Sons

This article is protected by copyright. All rights reserved.

is in keeping with that observed in other carnivores, with a stronger rostrocaudal gradient as compared to the dorsoventral gradient seen in primates.

Post-Hoc Diagnosis

Based on all clinical information, including histopathological analysis, three brains were determined to be from animals that had chronic DA toxicosis, and three from animals with no neurological signs or lesions (Table 1). Cases included in the DA group had hippocampal atrophy, gliosis, and neuronal loss or acute hippocampal neuronal necrosis consistent with lesions previously reported in sea lions exposed to DA (Silvangni et al., 2005). These designations were made by an experienced marine mammal veterinarian with extensive prior experience diagnosing and treating wild sea lions with DA toxicosis, in concert with an experienced veterinary histopathologist, and, given the availability of observation, brain imaging, and histopathology, they were made with a high degree of confidence. The three brains from animals with a post-hoc diagnosis of DA toxicosis had histologically identified neuronal loss and gliosis in the hippocampus (Fig. 3) and also had hippocampal atrophy per volumetry. The other three brains from sea lions without neurologic signs or lesions did not, and these three animals had received confident diagnoses of non-neurological conditions (Fig. 3). These brains were used as a DA and control group respectively, and all primary statistical comparisons were computed on these two groups. In two other cases, sea lions had evidence of cardiomyopathy often associated with DA but exhibited atypical neurological signs and/or hippocampal lesions were not completely consistent with DA toxicosis, so were analyzed separately. One brain (10840) had no histopathological signs of DA, but had age-related lesions, including axon loss with dilated axons sheaths and neuronal lipofuscinosis. This brain also exhibited hippocampal atrophy via volumetry. The other brain (10916) had lesions most severe in the amygdala with only very

This article is protected by copyright. All rights reserved.

Accepted Article

mild changes in the hippocampus. Amygdala lesions in this animal included marked gliosis, non-suppurative inflammation and mild neuronal necrosis (Figs. 3e and f). Mild widespread encephalitis was also identified throughout the brain. This brain exhibited no evidence of hippocampal atrophy. Neither brain, and neither animal, exhibited clear signs of chronic DA toxicosis as established in the veterinary literature.

Diffusion Measures

Probabilistic fornix tracings did not extend ventrally into the fimbria, likely due to termination of fibers traveling dorsal to the ventral boundary of the corpus callosum and due to thresholding (Fig 4). Because partial voluming effects complicate tractography in the fimbria (Concha et al., 2010), this was deemed acceptable. Although tracts did not survive into the fimbria, they were judged anatomically plausible representations of the body and pillar of the fornix for each subject. Pyramidal tracts proceeded from brainstem through rostral internal capsule (Fig. 4)

Although the cingulate was initially judged a promising target for tractography, due to its involvement in human epilepsy and relative ease of identification, cingulate fibers were extremely thin in all imaged brains, and could not be traced at reasonable diffusivity thresholds. This may be a feature of the pinniped brain, and bears further examination.

Two other tracts commonly examined in human epilepsy, the uncinate and arcuate fasciculi, have not been identified in the pinniped brain, and are defined by connection to cortical regions that have not been functionally delineated in the sea lion brain. These may also bear further examination.

Bayes Factors for comparisons of fornix FA values between control and DA brains were greater than 3 at each tract tracing threshold, indicating moderate or greater evidence for a meaningful

John Wiley & Sons

This article is protected by copyright. All rights reserved.

Accepted Article

difference between the two groups (5% threshold: 3.23 +/- 1.35; 10% threshold: 18.06 +/1 2.09; 20% threshold: 4.39 +/- 1.13). FA values were lower in the DA than control group (Fig.5) Bayes Factors for comparisons of fornix MD values between control and DA brains were between 1 and 2 at each tract tracing threshold, indicating slight anecdotal evidence for a meaningful difference between groups (5% threshold; 1.12 +/- 1.09; 10% threshold; 1.74 +/- 0.72; 20% threshold; 1.28 +/- 0.76) (Fig. 5). MD values were higher in the DA than the control group (Fig. 5). All Bayes Factors values for comparisons of pyramidal control tracts, for both FA and MD, were between 0.5 and 1, indicating slight anecdotal evidence for no difference between groups (5% threshold: FA, .60 +/- 1.02; MD, 0.66 +/- 0.53; 10% threshold: FA, 0.60 +/- 0.64; MD, 0.68 +/- 0.9; 20% threshold: FA, 0.82 +/- 1.82; MD, 0.80 +/- 2.16) (Fig. 5). Bayes Factor for the comparison between hippocampal-thalamic streamlines between control and DA brains was on the cusp between anecdotal and moderate evidence for a difference between groups (2.96 +/- 0.92) (Fig. 6).

CSL 10840, the brain with age-related neural signs but no evidence of DA toxicosis, had forniceal diffusion values more consistent with those of the DA animals than with the controls at all thresholds (more than 2 s.d. below the control mean and within 1 s.d. of the DA mean). CSL 10916, the brain with histopathological signs of DA in the amygdala but not the hippocampus, had forniceal diffusion values more consistent with those of the control brains than the DA brains at all thresholds tested (within 1 s.d. of the control mean, more than 2 s.d. greater than the DA mean).

John Wiley & Sons

This article is protected by copyright. All rights reserved.

Accepted Article

Discussion

In high-resolution post-mortem DTI, at three separate tracing thresholds, three sea lion brains with signs of chronic DA toxicosis (verified by clinical evaluation, histopathology, and hippocampal volumetrics) showed signs of reduced FA in the fornix in comparison to three brains with no neurological signs. The DA brains showed anecdotal evidence of increased MD at all three tracing thresholds. They also showed moderated signs of increased structural connectivity between the hippocampus and the thalamus. These findings are consistent with forniceal white matter pathology and increased hippocampal structural connectivity in animals with neurotoxic exposure to DA. This pattern has been observed with *in vivo* DTI assessment of human patients with MTL epilepsy (Concha et al., 2010; Otte et al., 2012; Dinkelacker et al., 2015). Together, these facts support the emerging characterization of DA toxicosis in sea lions as primarily an epileptic disease (Gulland and Ramsdell, 2014; Buckmaster et al., 2014).

Although the sample size in this study was small, including left and right diffusion values for only three DA and three control subjects, the apparent effects of DA toxicosis on white matter integrity in the fornix were notable, particularly as pertains to fractional anisotropy (FA, a measure of directional water flow in brain tissue). Apparent differences in mean diffusivity (MD, a measure of total, non-specific waterflow in brain tissue) were less clearly supported by Bayesian modeling. This may have been due to the higher variability in the MD measures than the FA and the small sample size. Alternatively, FA may be more affected in this population. Changes in FA are taken to be indicative of myelin degradation or reduction in axonal width (Cruces and Concha, 2015), while changes in MD tend to be associated with edema and necrosis. Typically, reduced FA and increased MD are seen at primary sites of neurological insult, while reduced FA with unaltered MD may be seen in secondary sites due to Wallerian degeneration

This article is protected by copyright. All rights reserved.

(Werring et al., 2000) In the current study, statistical modeling showed the greatest likelihood of difference between DA and control groups for both FA and MD at the 10% threshold, which, anecdotally, was the threshold that resulted in tract tracings most resembling those published previously in other species. Imaging and histopathology of fornix and other limbic tracts in larger samples of DA-affected sea lion brains are warranted. These may confirm the striking preliminary findings we report here, but also allow for more fine-grained analyses of the range of pathology experienced by wild animals with variable exposure histories.

Importantly, human data also indicate changes in white matter in other tracts, including the cingulate, and uncinate and arcuate fasciculi. Due to sparse fibers in the sea lion cingulate and lack of functional localization required to confidently identify cortico-cortical fiber tracts in the sea lion brain, we could not examine these tracts. Future work relying on histological identification (e.g., Sawyer, Turner & Kaas, 2016) and connectivity-based parcellation of cortical regions (e.g., Beckman, Johansen-Berg & Rushworth, 2009) in the sea lion brain would be of value. Of course, not all human tracts will have analogs in the brains of other mammals. For example, the arcuate fasiculus has been examined comparatively in ape and monkey brains, with notable differences (Rilling et al, 2008).

In addition to uncertainty about changes in other cortical tracts, we were unable to fully characterize exposure history and disease course in our subjects, as details on the animal's lives prior to stranding are unknown. This is a clear limitation of natural models in comparison to standard laboratory animal models. However, sea lions with DA toxicosis have been extensively studied in clinical settings, and this allows for confident and reliable diagnosis, particularly when structural brain imaging and post-mortem histology are available. While a number of naturally occurring conditions may lead to seizures or hippocampal damage, the histopathological

John Wiley & Sons

This article is protected by copyright. All rights reserved.

Accepted Article

characteristics of domoic acid exposure in sea lions have been well characterized in repeated studies (Silvagni et al. 2005; Goldstein et al. 2008). In the current study, the clinical history of each of our subjects was carefully considered before diagnosis.

While alternative and opportunistic models of epilepsy and DA toxicosis specifically, are not suited to fully replace more accessible and controlled rodent models, they may still be of great use, particularly as disease course in rodent models does not generalize particularly well to human epilepsy (Grone and Baraban, 2015). As a long-lived, large-bodied, large-brained wild mammal with a condition similar to human MTL epilepsy, sea lions with chronic DA toxicosis may represent an ecologically valid alternative model for human MTL epilepsy. As noted by Buckmaster et al. (2014), large numbers of wild sea lions are treated annually for DA toxicosis, during which time they might also receive experimental antiepileptogenic treatments. Novel therapies for sea lions affected by DA toxicosis could lead to improved outcomes and survivability in sea lions and be a model for human epilepsy treatments. Importantly, wild sea lions in the rehabilitation setting may suffer from multiple medical conditions—it is difficult to fully control for confounding variables. However, in this, a free ranging animal may better mirror the human medical population than do most laboratory models. In addition, the clear diagnostic distinction between acute exposure and the chronic resulting condition (Goldstein et al. 2008) allows for clinical selection of animals with appropriate disease characteristics, even in a rehabilitation setting.

Post-mortem DTI also shows promise for better characterizing the specific network effects of DA toxicosis and resultant chronic MTL epilepsy. Large numbers of sea lions are euthanized each year with intractable DA toxicosis, many with full veterinary workups and diagnoses, so a large number of brains may be imaged opportunistically to better understand the neurobiological

This article is protected by copyright. All rights reserved.

Accepted Article

effects of the disease. This approach may be of particular use in examining the developmental effects of DA exposures. It's known that sea lion fetuses are exposed to DA *in utero* when pregnant mothers receive high enough doses of the toxin (Ramsdell and Zabka, 2008), but the long-term neural effects of this are unknown. In addition, it's been shown that DA-related hippocampal pathology worsens with age in sea lions (Montie et al., 2012). In both cases, opportunistic examinations of white matter pathology and brain connectivity may better characterize the impact of exposure across the lifespan. Such studies are limited by incomplete patient histories, but due to tagging, rehabilitation, and rerelease, a number of animals are available for repeated behavioral testing, and disease course can be partially inferred from animal's age and neuropathology.

The current findings also extend our understanding of the likely neurobehavioral effects of DA toxicosis in wild sea lions. Cruces and Concha (2015) have characterized epilepsy as primarily a brain network disease, as opposed to a limited focal brain disorder. Alterations across brain networks will have notable effects on cognitive and behavioral processes in animals afflicted with epilepsy. Prior evidence in wild sea lions with DA toxicosis showed disrupted functional connectivity between the hippocampus and the thalamus as well as spatial memory deficits (Cook et al., 2015). Our finding of altered white matter characteristics of the fornix and potentially increased structural connectivity between the hippocampus and thalamus in sea lions with DA toxicosis expand our understanding of the neurobehavioral effects of DA toxicosis. The fornix is one of the primary pathways from the hippocampus to the thalamus (Aggleton et al., 2010), and this pathway is known essential for supporting episodic and spatial memory (Aggleton, Neave, Nagle and Hunt, 1995; Aggleton and Brown, 1999). Structural damage to this pathway can lead to severe amnesic symptoms in humans and rodents, which could be highly

This article is protected by copyright. All rights reserved.

Accepted Article

Accepted Article

maladaptive for flexible central-place foragers such as sea lions. Interestingly, reduced forniceal FA in human patients has not been previously associated with specific memory deficits; rather, it has been linked with deficits in processing speed (McDonald et al., 2008; Alexander et al., 2014), suggesting a novel line of behavioral testing with DA-exposed sea lions.

Opportunistic post-mortem DTI may be a generally useful technique for probing the effects of environmental exposures and naturally occurring neural conditions. This was highlighted in the present study by identification of two brains with neurological signs not consistent with the typical presentation of DA toxicosis. These were treated as provisional case studies. One showed histopathological signs of DA toxicosis in the amygdala, but not the hippocampus. This animal had no hippocampal atrophy and no signs of fornix pathology. DA has been shown to target the amygdala, but has not typically been seen to do so exclusive of the hippocampus (Silvagni et al., 2005). If the insult to the amygdala in this brain was DA-related, this suggests a novel disease presentation bearing further examination.

Another brain had potentially age-related brain lesions, hippocampal atrophy, and altered forniceal diffusion, but no clear signs of DA toxicosis. Pathological aging in humans has been shown to cause hippocampal atrophy and forniceal pathology (Jack et al., 2000; Rose et al., 2000; Acosta et al., 2010). Notably, age-related neuropathology can result in seizures in humans (Romanelli et al. 1990) and in mouse models of neurobiological aging (Palop et al. 2007), which could complicate attempts to differentiate insult from normal aging versus long-term effects of DA exposure. A number of other conditions may also lead to hippocampal damage and epilepsy, including conditions involving encephalitis such as anti-AMPAR (Lancaster, Martinez-Hernandez & Dalmau, 2011). Nonetheless, the anecdotal finding of potential age-related neural changes in a wild sea lions is intriguing, and raises the possibility that opportunistic post-mortem

This article is protected by copyright. All rights reserved.

imaging might be used to study ecologically valid models of neural aging in large-brained, long-lived mammals, not practically done in the laboratory setting in any reasonable time-frame. Importantly, it also suggests that age-related changes may interact with DA-related changes in the wild sea lion brain.

Naturally occurring exposure to DA is an increasing threat to wild animals and potentially to humans (McCabe et al. 2016; Ferriss et al. 2017). Opportunistic post-mortem DTI can help characterize the effect of this toxin in a range of otherwise inaccessible species. Findings may also further the use of natural models for epilepsy. More generally, post-mortem DTI allows neurological assessment of a great many species not typically studied, and may increase understanding of naturally occurring disease processes as well as comparative neurobiology. Given success in obtaining in vivo MRI and fMRI measures in anesthetized sea lions (Cook et al. 2015), future studies might also attempt to obtain in vivo DTI measures from animals in a rehabilitation setting. This could broaden the range of available subjects, and, in certain circumstances, allow for longitudinal assessment of specific neural tracts. Such data could meaningfully inform work conducted with post-mortem brains, and vice versa.

Acknowledgements: The authors thank Karla Miller, Sean Foxley and Saad Jbabdi of Oxford University for support in sequence implementation and data analysis. The authors further thank the veterinary pathology team at The Marine Mammal Center for support in specimen acquisition. Imaging data acquisition was supported by an internal FERN grant to P.F.C. The authors declare no competing financial interests.

This article is protected by copyright. All rights reserved.

Accepted Article

Accepted Article

Conflict of Interest Statement: None of the authors report any conflicts of interest.

Role of Authors: All authors had full access to all the data in the study and take responsibility for the integrity of the data and the accuracy of the data analysis. Study concept and design: PC, GB, FG. Acquisition of data: PC, GB, KC, SJ. Analysis and interpretation of data: PC, SJ, KC. Drafting of the manuscript: PC. Critical revision of the manuscript for important intellectual content: PC. Statistical analysis: PC.

Literature Cited

Acosta-Cabronero J, Williams GB, Pengas G, Nestor PJ. 2010. Absolute diffusivities define the landscape of white matter degeneration in Alzheimer's disease. Brain 133(2):529-39.

Aggleton JP, Brown MW. 1999. Episodic memory, amnesia, and the hippocampal–anterior thalamic axis. Behav Brain Sci 22(03):425-44.

Aggleton JP, Neave N, Nagle S, Hunt PR. 1995. A comparison of the effects of anterior thalamic, mamillary body and fornix lesions on reinforced spatial alternation. Behav Brain Sci 68(1):91-101.

Aggleton JP, O'Mara SM, Vann SD, Wright NF, Tsanov M, Erichsen JT. 2010. Hippocampal–anterior thalamic pathways for memory: uncovering a network of direct and indirect actions. Eur J Neurosci 31(12):2292-307.

This article is protected by copyright. All rights reserved.

Alexander RP, Concha L, Snyder TJ, Beaulieu C, Gross DW. 2014. Correlations between Limbic White Matter and Cognitive Function in Temporal-Lobe Epilepsy, Preliminary Findings. Front Aging Neurosci 6:142.

Anderson DM, Burkholder JM, Cochlan WP, Glibert PM, Gobler CJ, Heil CA, Kudela RM, Parsons ML, Rensel JJ, Townsend DW, Trainer VL. 2008. Harmful algal blooms and eutrophication: examining linkages from selected coastal regions of the United States. Harmful Algae 8(1):39-53.

Behrens TE, Woolrich MW, Jenkinson M, Johansen-Berg H, Nunes RG, Clare S, Matthews PM, Brady JM, Smith SM. 2003. Characterization and propagation of uncertainty in diffusion-weighted MR imaging. Magn Reson Med 50(5):1077-88.

Beckmann, M., Johansen-Berg, H., & Rushworth, M. F. 2009. Connectivity-based parcellation of human cingulate cortex and its relation to functional specialization. Journal of Neuroscience, 29(4), 1175-1190.

Behrens TE, Berg HJ, Jbabdi S, Rushworth MF, Woolrich MW. 2007. Probabilistic diffusion tractography with multiple fibre orientations: What can we gain? Neuroimage 34(1):144-55.

Bernabeu R, Sharp FR. 2000. NMDA and AMPA/kainate glutamate receptors modulate dentate neurogenesis and CA3 synapsin-I in normal and ischemic hippocampus. J Cerebr Blood F Met 20(12):1669-80.

Berns GS, Cook PF, Foxley S, Jbabdi S, Miller KL, Marino L. 2015. Diffusion tensor imaging of dolphin brains reveals direct auditory pathway to temporal lobe. Proc R Soc B 282(1811):1203.

This article is protected by copyright. All rights reserved.

Bonilha L, Nesland T, Martz GU, Joseph JE, Spampinato MV, Edwards JC, Tabesh A. 2012. Medial temporal lobe epilepsy is associated with neuronal fibre loss and paradoxical increase in structural connectivity of limbic structures. J Neurol Neurosur PS jnnp-2012.

Buckmaster PS, Wen X, Toyoda I, Gulland F, Van Bonn W. 2014. Hippocampal neuropathology of domoic acid–induced epilepsy in California sea lions (Zalophus californianus). J Comp Neurol 522(7):1691-706.

Buxton RB. 1993. The diffusion sensitivity of fast steady-state free precession imaging. Magn Reson Med 29(2):235-43.

Catani M, Jones DK, Donato R. 2003. Occipito-temporal connections in the human brain. Brain 126(9):2093-107

Cook PF, Reichmuth C, Gulland F. 2011. Rapid behavioural diagnosis of domoic acid toxicosis in California sea lions. Biol Let (UK) 7(4):536-8.

Cook PF, Reichmuth C, Rouse AA, Libby LA, Dennison SE, Carmichael OT, Kruse-Elliott KT, Bloom J, Singh B, Fravel VA, Barbosa L, Stuppino JL, Van Bonn W, Gulland F, Ranganath C. 2015. Algal toxin impairs sea lion memory and hippocampal connectivity, with implications for strandings. Science 350(6267):1545-7.

Cook PF, Reichmuth C, Rouse A, Dennison S, Van Bonn B, & Gulland F. (2016). Natural exposure to domoic acid causes behavioral perseveration in Wild Sea lions: Neural underpinnings and diagnostic application. Neurotoxicology and Teratology 57: 95-105.

Concha L, Livy DJ, Beaulieu C, Wheatley BM, Gross DW. 2010. In vivo diffusion tensor imaging and histopathology of the fimbria-fornix in temporal lobe epilepsy. J Neurosci 30(3):996-1002.

This article is protected by copyright. All rights reserved.

Rodríguez-Cruces R, & Concha L. 2015. White matter in temporal lobe epilepsy: clinico-pathological correlates of water diffusion abnormalities. Quantitative imaging in medicine and surgery, 5(2), 264.

Dakshinamurti K, Sharma SK, Sundaram M. 1991. Domoic acid induced seizure activity in rats. Neurosci Lett 127(2):193-7.

Dinkelacker V, Valabregue R, Thivard L, Lehéricy S, Baulac M, Samson S, Dupont S. 2015. Hippocampal-thalamic wiring in medial temporal lobe epilepsy: Enhanced connectivity per hippocampal voxel. Epilepsia 56(8):1217-26.

Dugladze, T., Vida, I., Tort, A. B., Gross, A., Otahal, J., Heinemann, U., ... & Gloveli, T. 2007. Impaired hippocampal rhythmogenesis in a mouse model of mesial temporal lobe epilepsy. Proceedings of the National Academy of Sciences 104(44):17530-17535.

Ferriss B E, Marcinek D J, Ayres D, Borchert J, & Lefebvre KA. 2017. Acute and chronic dietary exposure to domoic acid in recreational harvesters: A survey of shellfish consumption behavior. Environment International 101:70-79.

Goldstein T, Mazet JA, Zabka TS, Langlois G, Colegrove KM, Silver M, Bargu S, Van Dolah F, Leighfield T, Conrad PA, Barakos J. 2008. Novel symptomatology and changing epidemiology of domoic acid toxicosis in California sea lions (Zalophus californianus): an increasing risk to marine mammal health. P Roy Soc B-Biol Sci 275(1632):267-76.

Govindan RM, Makki MI, Sundaram, S K, Juhász C, & Chugani HT. 2008. Diffusion tensor analysis of temporal and extra-temporal lobe tracts in temporal lobe epilepsy. Epilepsy research 80(1);30-41.

John Wiley & Sons

This article is protected by copyright. All rights reserved.

Greig DJ, Gulland F, and Kreuder C. 2005. A decade of live California sea lion (Zalophus californianus) strandings along the central California coast: causes and trends, 1991-2000. Aquatic Mammals 31(1):40-51.

Grone BP, Baraban SC. 2015. Animal models in epilepsy research: legacies and new directions. Nat Neurosci 18(3):339-43.

Gross DW. 2011. Diffusion tensor imaging in temporal lobe epilepsy. Epilepsia 52(s4):32-4.

Gulland FM, Haulena M, Fauquier D, Langlois G, Lander ME, Zabka T, Duerr R. 2002. Domoic acid toxicity in Californian sea lions (Zalophus californianus): clinical signs, treatment and survival. Vet Rec 150(15):475-80.

Gulland FMD., Hall AJ, Greig DJ, Frame ER, Colegrove KM, Booth RKN, Wasser SK, Scott-Moncrieff JCR. 2012. Evaluation of circulating eosinophil count and adrenal gland function in California sea lions naturally exposed to domoic acid. Journal of the American Veterinary Medical Association 241(7): 943-949.

Gutman DA, Keifer OP, Magnuson ME, Choi DC, Majeed W, Keilholz S, Ressler KJ. 2012. A DTI tractography analysis of infralimbic and prelimbic connectivity in the mouse using high-throughput MRI. Neuroimage 63(2):800-11.

Guye M, Parker GJ, Symms M, Boulby P, Wheeler-Kingshott CA, Salek-Haddadi A, Barker GJ, Duncan JS. 2003. Combined functional MRI and tractography to demonstrate the connectivity of the human primary motor cortex in vivo. Neuroimage 19(4):1349-60.

Hadfield JD. 2010. MCMC methods for multi-response generalized linear mixed models: the MCMCglmm R package. Journal of Statistical Software 33(2):1-22.

This article is protected by copyright. All rights reserved.

Hiolski EM, Ito S, Beggs JM, Lefebvre KA, Litke AM, & Smith DR. 2016. Domoic acid disrupts the activity and connectivity of neuronal networks in organotypic brain slice cultures. Neurotoxicology 56:215-224.

Jack CR, Petersen RC, Xu Y, O'brien PC, Smith GE, Ivnik RJ, Boeve BF, Tangalos EG, Kokmen E. 2000. Rates of hippocampal atrophy correlate with change in clinical status in aging and AD. Neurology 55(4):484-90.

Jeffery B, Barlow T, Moizer K, Paul S, Boyle C. 2004. Amnesic shellfish poison. Food and Chemical Toxicology 42(4):545-57.

Kirkley KS, Madl JE, Duncan C, Gulland FM, & Tjalkens RB. 2014. Domoic acid-induced seizures in California sea lions (Zalophus californianus) are associated with neuroinflammatory brain injury. Aquatic Toxicology156:259-268.

Kola I, Landis J. 2004. Can the pharmaceutical industry reduce attrition rates? Nature Reviews Drug Discovery 3(8):711-6.

Lancaster, E., Martinez-Hernandez, E., & Dalmau, J. 2011. Encephalitis and antibodies to synaptic and neuronal cell surface proteins. Neurology 77(2):179-189.

Liao W, Zhang Z, Pan Z, Mantini D, Ding J, Duan X, Luo C, Lu G, Chen H. 2010. Altered functional connectivity and small-world in mesial temporal lobe epilepsy. PloS one 5(1):e8525.

Lee MD, & Wagenmakers EJ. 2013. Bayesian data analysis for cognitive science: A practical course.

Lefebvre KA, Robertson A, Frame ER, Colegrove KM, Nance S, Baugh KA, ... & Gulland FM. (2010). Clinical signs and histopathology associated with domoic acid poisoning in northern fur

This article is protected by copyright. All rights reserved.

seals (Callorhinus ursinus) and comparison of toxin detection methods. Harmful Algae 9(4):374-383.

Lefebvre KA, Robertson A.2010. Domoic acid and human exposure risks: a review. Toxicon 56(2):218-30.

Lefebvre KA, Quakenbush L, Frame E, Huntington KB, Sheffield G, Stimmelmayr R, Bryan A, Kendrick P, Ziel H, Goldstein T, Snyder JA. 2016. Prevalence of algal toxins in Alaskan marine mammals foraging in a changing arctic and subarctic environment. Harmful Algae 55:13-24.

Lothman EW, Collins RC. 1981. Kainic acid induced limbic seizures: metabolic, behavioral, electroencephalographic and neuropathological correlates. Brain Res 218(1):299-318.

McCabe RM, Hickey BM, Kudela RM, Lefebvre KA, Adams NG, Bill BD, ... & Trainer VL. 2016. An unprecedented coastwide toxic algal bloom linked to anomalous ocean conditions. Geophysical Research Letters 43(19).

McDonald CR, Ahmadi ME, Hagler DJ, Tecoma ES, Iragui VJ, Gharapetian L, Dale AM, Halgren E. 2008. Diffusion tensor imaging correlates of memory and language impairments in temporal lobe epilepsy. Neurology 71:1869-76.

McNab JA, Jbabdi S, Deoni SC, Douaud G, Behrens TE, Miller KL. 2009. High resolution diffusion-weighted imaging in fixed human brain using diffusion-weighted steady state free precession. Neuroimage 46(3):775-85.

Miller KL, Stagg CJ, Douaud G, Jbabdi S, Smith SM, Behrens TE, Jenkinson M, Chance SA, Esiri MM, Voets NL, Jenkinson N. 2011. Diffusion imaging of whole, post-mortem human brains on a clinical MRI scanner. Neuroimage 57(1):167-81.

This article is protected by copyright. All rights reserved.

Miller KL, McNab JA, Jbabdi S, Douaud G. 2012. Diffusion tractography of post-mortem human brains: optimization and comparison of spin echo and steady-state free precession techniques. Neuroimage 59(3):2284-97.

Mishra AM, Bai H, Gribizis A, Blumenfeld H. 2011. Neuroimaging biomarkers of epileptogenesis. Neuroscience Letters 497(3):194-204.

Montie EW, Pussini N, Schneider GE, Battey TW, Dennison S, Barakos J, Gulland F. 2009. Neuroanatomy and volumes of brain structures of a live California sea lion (Zalophus californianus) from magnetic resonance images. Anatomical Record 292(10):1523-47.

Montie EW, Wheeler E, Pussini N, Battey TW, Barakos J, Dennison S, Colegrove K, Gulland F. 2010. Magnetic resonance imaging quality and volumes of brain structures from live and postmortem imaging of California sea lions with clinical signs of domoic acid toxicosis. Diseases of Aquatic Organisms 91(3):243-56.

Montie EW, Wheeler E, Pussini N, Battey TW, Van Bonn W, Gulland F. 2012. Magnetic resonance imaging reveals that brain atrophy is more severe in older California sea lions with domoic acid toxicosis. Harmful Algae 20:19-29.

Morey RD, Rouder JN, & Jamil T. 2015. BayesFactor: Computation of Bayes factors for common designs. *R package version 0.9*, *9*.

Muha N, Ramsdell JS. 2011. Domoic acid induced seizures progress to a chronic state of epilepsy in rats. Toxicon 57(1):168-71.

Otte WM, van Eijsden P, Sander JW, Duncan JS, Dijkhuizen RM, Braun KP. 2012. A meta-analysis of white matter changes in temporal lobe epilepsy as studied with diffusion tensor imaging. Epilepsia 53(4):659-67.

This article is protected by copyright. All rights reserved.

Palop, J J, Chin J, Roberson ED, Wang J, Thwin, MT, Bien-Ly N, ... & Finkbeiner S. 2007. Aberrant excitatory neuronal activity and compensatory remodeling of inhibitory hippocampal circuits in mouse models of Alzheimer's disease. Neuron 55(5):697-711.

Perl TM, Bédard L, Kosatsky T, Hockin JC, Todd EC, Remis RS. 1990. An outbreak of toxic encephalopathy caused by eating mussels contaminated with domoic acid. New England Journal of Medicine 322(25):1775-80.

Pierpaoli C, Barnett A, Pajevic S, et al. 2001. Water diffusion changes in Wallerian degeneration and their dependence on white matter architecture. Neuroimage 13:1174–1185.

Pulido OM. 2008. Domoic acid toxicologic pathology: a review. Marine Drugs 6(2):180-219.

Ramsdell JS, Zabka T. 2008. In utero domoic acid toxicity: a fetal basis to adult disease in the California sea lion (Zalophus californianus). Marine Drugs 6(2):262-90.

Ramsdell JS, Gulland FM. 2014. Domoic acid epileptic disease. Marine Drugs 12(3):1185-207.

Rose SE, Chen F, Chalk JB, Zelaya FO, Strugnell WE, Benson M, Semple J, Doddrell DM. 2000. Loss of connectivity in Alzheimer's disease: an evaluation of white matter tract integrity with colour coded MR diffusion tensor imaging. Journal of Neurology, Neurosurgery & Psychiatry 69(4):528-30.

Rilling, JK, Glasser MF, Preuss TM, Ma X, Zhao T, Hu X, & Behrens TE. 2008. The evolution of the arcuate fasciculus revealed with comparative DTI. Nature Neuroscience 11(4):426.

Romanelli MF, Morris JC, Ashkin K, & Coben LA. 1990. Advanced Alzheimer's disease is a risk factor for late-onset seizures. Archives of Neurology 47(8):847-850.

Rouder, JN, Morey, RD, Speckman PL, Province JM, 2012. Default Bayes Factors for ANOVA Designs. Journal of Mathematical Psychology 56:356-374.

This article is protected by copyright. All rights reserved.

Sawyer EK, Turner EC, & Kaas J H 2016. Somatosensory brainstem, thalamus, and cortex of the California sea lion (Zalophus californianus). Journal of Comparative Neurology 524(9):1957-1975.

Scholin CA, Gulland F, Doucette GJ, Benson S, Busman M, Chavez FP, Cordaro J, DeLong R, De Vogelaere A, Harvey J, Haulena M. 2000. Mortality of sea lions along the central California coast linked to a toxic diatom bloom. Nature, 403(6765), 80-4.

Silvagni PA, Lowenstine LJ, Spraker T, Lipscomb TP, Gulland FM. 2005. Pathology of domoic acid toxicity in California sea lions (Zalophus californianus). Veterinary Pathology 42(2):184-91.

Silver MW, Bargu S, Coale SL, Benitez-Nelson CR, Garcia AC, Roberts KJ, Sekula-Wood E, Bruland KW, Coale KH. 2010. Toxic diatoms and domoic acid in natural and iron enriched waters of the oceanic Pacific. Proceedings of the National Academy of Sciences USA 107(48):20762-7.

Thomas K, Harvey JT, Goldstein T, Barakos J, Gulland F. 2010. Movement, dive behavior, and survival of California sea lions (Zalophus californianus) posttreatment for domoic acid toxicosis. Marine Mammal Science 26(1):36-52.

Thomas C, Frank QY, Irfanoglu MO, Modi P, Saleem KS, Leopold DA, Pierpaoli C. 2014. Anatomical accuracy of brain connections derived from diffusion MRI tractography is inherently limited. Proceedings of the National Academy of Sciences USA 111(46):16574-9.

Yeh FC, Verstynen TD, Wang Y, Fernández-Miranda JC, Tseng WY. 2013. Deterministic diffusion fiber tracking improved by quantitative anisotropy. PloS one 8(11):e80713.

Wakana S, Jiang H, Nagae-Poetscher LM, Van Zijl PC, Mori S. 2004. Fiber tract–based atlas of human white matter anatomy 1. Radiology 230(1):77-87.

John Wiley & Sons

This article is protected by copyright. All rights reserved.

Waites AB, Briellmann RS, Saling MM, Abbott DF, Jackson GD. 2006. Functional connectivity networks are disrupted in left temporal lobe epilepsy. Annals of Neurology 59(2):335-43.

Werring DJ, Toosy AT, Clark CA, et al. 2000. Diffusion tensor imaging can detect and quantify corticospinal tract degeneration after stroke. J Neurol Neurosurg Psychiatry, 69:269–272.

Zabka TS, Goldstein T, Cross C, Mueller RW, Kreuder-Johnson C, Gill S, Gulland FMD. 2009. Characterization of a degenerative cardiomyopathy associated with domoic acid toxicity in California sea lions (Zalophus californianus). Veterinary Pathology 46: 105-119.

Zhao Y, Staudenmayer J, Coull BA, Wand MP.2006. "General design Bayesian generalized linear mixed models." Statistical Science 21(1):35–51.

Figure 1: Hippocampal and Thalamic Regions of Interest. Representative ROIs from one control subject, 10814. ROIs were drawn using FSL's FSLView in the transverse plane. Hippocampal ROIs were drawn directly on trufi images. Thalamic ROIs were drawn on B0 images and transformed to trufi space for visualization. a) Three representative hippocampal tracings from along the longitudinal axis of the hippocampus, shown at left. The red transects show tracings on a dorsocaudal slice, just ventral to the splenium (top), a slice from the middle of the hippocampus adjacent and lateral to the inferior colliculi (middle), and a ventrorostral slice, adjacent and lateral to the interpeduncular fossa (bottom). Left hippocampal regions are shown in red (on the right side of the image in radiological presentation), and right regions are left bare for visualization. b) Right thalamus is shown (on the left side of each image) in three

John Wiley & Sons

This article is protected by copyright. All rights reserved.

Accepted Article

imaging planes, transverse (left), sagittal (middle), and coronal (right). Thalamus was traced bilaterally in one mask, but left thalamus is uncovered here for purposes of visualization.

Figure 2: Deterministic Tract Renderings of Whole Brain and Fornix. Representative tract renderings from one control subject, 10814, produced in DSI studio. a) Whole brain rendering of sea lion white matter tracts. Viewed in the transverse plane, ventral to the brain, with rostral portion at the top of the image. Tract color represents fiber direction: green=rostral-caudal, red=left-right, blue=dorsal-ventral. The fornix is clearly visible as an inverted green "v", just caudal to the genu of the corpus callosum (large left-right red fiber bundle). The blue tip of the "v" is where the fornix takes its ventral turn into the pillar. The pyramidal tract is also visible, exiting the brain stem dorsal to the pons before heading rostrolaterally through the internal capsule to motor cortex (which is notably more rostral in the carnivore than primate brain). b) A fornix tracing including fimbria. This tracing was produced with a spherical seed centered on the crus of the fornix, in the same location as used to seed probabilistic tracings in FSL. Planar termination masks were placed caudal to the septum pellucidum, just ventral to the splenium, and lateral to the hippocampus. QA threshold had to be lowered (0.07) to trace into fimbria.

Figure 3: Hematoxylin and eosin stained sections of brain from sea lions illustrating histological lesions characteristic of typical and atypical DA toxicosis. a) Hippocampus from a normal California sea lion (case 11141). DG = Dentate gyrus; CA = cornu ammonis. Bar = 500 µm. b) Higher power image of the hippocampus from case 11141. Note the normal hippocampal neurons (arrows). Bar = 50 µm. c) Hippocampus from a sea lion with domoic acid toxicosis (case 11217). Note the hippocampal atrophy, loss of neurons in the dentate

This article is protected by copyright. All rights reserved.

Accepted Article

gyrus (DG) and cornu ammonis (CA), and the increased numbers of glial cells. Bar = 500 µm. d) Higher power image of the dentate gyrus from case 11217. Note the hypereosinophilic necrotic neurons (arrows) and gliosis. Bar = 20 µm. e) Photomicrograph of the amygdala from case 10916. There is severe gliosis and inflammation. Box denotes area of high power image (f). Bar = 200 µm. f) Higher power image of the amygdala from case 10916 illustrating gliosis and perivascular chuffing with lymphocytes. Bar = 20 µm. g) Normal amygdala from case 10840. Box denotes area of high power image (h). Bar = 200 µm. h) High power image of normal amygdala. Note the small amount of light yellow lipofuscin within neurons associated with older age. Bar = 50 µm.

Figure 4: Probabilistic Fornix and Pyramidal Tract Tracings. Representative tracings from one control subject, 10814. Tracts were computed in diffusion space, then transformed for visual presentation in high-resolution trufi space. a) Right (red) and left (blue) fornix tracings in the transverse, sagittal, and coronal plane, from left to right. b) Right (red) and left (blue) pyramidal tract tracings in the transverse, sagittal, and coronal plane from left to right. In both a and b, right and left tracts were traced independently from separate seeds. Tracings are thresholded at 10% of streamlines, i.e., only voxels receiving 10% or more of the streamlines traced from the seed are shown.

Figure 5: Lower Directional Diffusion in the Fornix of a DA Brain. Fornix was traced in DSI studio using the same seed as discussed in the caption of Figure 3, but with a higher qa threshold (0.10). Color represents qa value (analogous to FA), as demonstrated in color scale bars, with

This article is protected by copyright. All rights reserved.

Accepted Article

warmer colors representing higher qa/greater directional water diffusion. a) Representative right fornix render in a control animal, 10814, shown in a sagittal slice over the FA map (left) and in a head-on coronal view extracted (right). Higher directional diffusion can be seen in the crus of the fornix represented by bright yellow. b) Representative right fornix render in a DA animal, 11182, with clearly lower directional diffusion over the crus represented by deeper red. c) Mean FA (left column) and MD (right column) are shown on the y axis in the pyramidal (top row) and fornix (bottom row) tracts for each control and DA subject. Right and left values for each animal are shown separately. Pairs of values (right and left) for each animal are coded in the figure by shape. FA and MD values were extracted from binarized masks at the 10% by-voxel threshold. MD values have been multiplied by 1000 for presentation purposes. Plots show mean, 25th and 75th percentile within each box, with whiskers extending to the highest and lowest values within 1.5 * the inter-quartile range. Pyramidal diffusion measures were not distinct between DA and control brains. Forniceal FA was decreased and MD increased in DA brains, indicative of white-matter pathology. d) Side views of right and left fornix for each subject, as computed in FSL. These are thresholded at 10% by-voxel, and represent the FA values in the 10% by-voxel thresholds masked regions. Here, color represents FA value, with higher values (greater directionality) represented as yellow.

Figure 6: Higher Hippocampal-Thalamic Structural Connectivity in DA Brains. Number of total streamlines between right and left hippocampus and bilateral thalamus, corrected by size of hippocampal and thalamic masks, are shown for each control and DA animal. Right and left values for each animal are combined within the same box, although statistics were computed by repeated-measures ANOVA. Pairs of values (right and left) for each animal are coded in the

This article is protected by copyright. All rights reserved.

figure by shape. Plots show mean, 25th and 75th percentile within each box, with whiskers extending to the highest and lowest values within 1.5 * the inter-quartile range.

Movie 1: Rotation of Whole Brain Deterministic Rendering of White Matter Pathways in a Control Sea Lion. Major white matter pathways at a qa threshold of 0.10. Green fibers are rostrocaudal, red are left-right, and blue are dorsoventral.

Movie 2: Rotation of Deterministic Corpus Callosum Render. Right corpus callosum of one control subject, 10814, traced as described in caption to Figure 3, shown here in green, was overlaid with a whole-brain render of white matter tracts (dark purple) and rotated for the purpose of visualization.

Accepted Article

This article is protected by copyright. All rights reserved.

Accepted Article

Title: Post-Mortem DTI Reveals Altered Hippocampal Connectivity in Wild Sea Lions Diagnosed with Chronic Toxicosis from Algal Exposure

Authors: Peter F. Cook,[1,2] Gregory S. Berns,[2] Kathleen Colegrove,[3] Shawn Johnson,[4] Frances Gulland[4]

Affiliations: 1. Long Marine Lab, University of California Santa Cruz, 95060, USA 2. Department of Psychology, Emory University, 30322, USA 3. College of Veterinary Medicine, University of Illinois at Urbana-Champaign, 60513, USA 4. The Marine Mammal Center, Sausalito, CA, 94965 USA

Abbreviated Title: Altered Hippocampal Connectivity in Wild Sea Lions

Requested Associate Editor: Oswald Steward

Key Words: Domoic Acid, Diffusion Tensor Imaging, Fornix, Sea Lions, Epilepsy

Corresponding author: Peter F. Cook, pcook930@gmail.com, 831-535-2686, New College Florida, Sarasota, FL 34234

This article is protected by copyright. All rights reserved.

Accepted Article

Abstract

Hundreds of wild California sea lions (*Zalophus californianus*) exposed to the algal neurotoxin domoic acid are treated in veterinary rehabilitation centers each year. Common chronic effects of toxic exposure in these animals are seizures and hippocampal damage, and they have been proposed as a natural animal model for human epilepsy. Humans with medial temporal lobe epilepsy present with white matter pathology in a number of tracts including the fornix and increased structural connectivity between the hippocampus and thalamus. However, there are no prior data on structural connectivity in sea lion brains, with or without neuropathology. In the present study, we used a novel diffusion tensor imaging technique to obtain high resolution (1mm isotropic) white matter maps in brains obtained opportunistically post-mortem from wild sea lions with and without chronic clinical signs of toxic exposure to domoic acid. All animals had received a full veterinary workup and diagnosis prior to euthanasia. We measured hippocampal atrophy morphometrically, and all brains were examined histopathologically. In animals diagnosed with chronic domoic acid toxicosis, the fornix showed signs of altered diffusion properties indicative of pathology; these brains also had increased structural connectivity between hippocampus and thalamus in comparison to brains from animals with no neurological signs. These findings establish further parallels between human medial temporal lobe epilepsy and a naturally occurring condition in wild sea lions and simultaneously advance general knowledge of the deleterious effects of an increasingly common natural toxin.

Introduction

John Wiley & Sons

This article is protected by copyright. All rights reserved.

Accepted Article

Each year along the West coast, hundreds of sea lions are exposed in the wild to algal neurotoxin domoic acid (DA), come to shore in distress (i.e., strand), and are taken to veterinary rehabilitation facilities (Scholin et al., 2000; Goldstein et al., 2008). DA, the cause of "amnesic shellfish poisoning" in humans (Perl et al., 1990), binds preferentially to α-amino-3-hydroxy-5-methyl-4-isoxazolepropionic acid (AMPA) and kainate receptors (Silvagni et al., 2005), which are plentiful in mammalian hippocampus (Bernabeu and Sharp, 2000). Affected sea lions have been extensively studied in veterinary rehabilitation settings. Acute exposure in sea lions leads to excitotoxic cell death in the dentate gyrus and CA3 portion of the hippocampus (Pullido, 2008), and can cause seizures and death. Sea lions who survive initial exposure may develop chronic epilepsy and resultant hippocampal atrophy (Goldstein et al., 2008, Montie et al., 2010). They have also been shown to have potentially maladaptive spatial memory deficits and behavioral perseveration (Cook et al., 2011; Cook et al., 2015; Cook et al. 2016), disrupted navigation (Thomas et al., 2010), increased likelihood of restranding after release, and, in most cases, eventual mortality (Gulland et al., 2002). This chronic condition is recognized as a differentiable clinical diagnosis in wild sea lions with clear behavioral and pathophysiological correlates (Goldstein et al. 2008).

Both DA and kainic acid are used to produce laboratory models of seizure disorders (Lothman and Collins, 1981; Dakshinamurti et al., 1991), and the chronic effects of naturally occurring DA exposure in sea lions have been suggested to be largely analogous to medial temporal lobe (MTL) epilepsy in humans (Muha and Ramsdell, 2011; Ramsdell and Gulland, 2014). Like humans with MTL epilepsy, sea lions with DA toxicosis show cell death and mossy fiber sprouting in the dentate gyrus, and typically unilateral patterns of gross hippocampal atrophy. Due to these similarities, wild sea lions exposed to DA have been proposed as an accessible and

This article is protected by copyright. All rights reserved.

Accepted Article

ecologically valid alternative medical model for human epilepsy (Buckmaster et al., 2014; Grone and Baraban, 2015). However, further study is needed to chart the extent of neurobiological effects of toxic exposure in wild sea lions, both for the sake of improving clinical treatment and assessing the validity of sea lions as a comparative model for disease.

In diffusion tensor imaging (DTI) studies, humans with MTL epilepsy show distributed white matter pathology, typically presenting as decreased fractional anisotropy (FA) and, in certain cases, increased mean diffusivity (MD), in a number of limbic pathways. Meta-analyses suggest damage is most pronounced in limbic tracts and those passing through the temporal lobe, including the fornix, cingulate, arcuate fasciculus, and uncinate fasciculus (Gross et al., 2011; Mishra et al., 2011; Otte et al. 2012; Govindan et al. 2008). Joint imaging and histology work in humans have linked decreased FA with decreased fiber bundle circumference and reduced myelination (Werring et al., 2000; Pierpaoli et al., 2001; Concha et al., 2010; Cruces & Concha, 2015). MTL epilepsy has also been shown to increase hippocampal structural connectivity (Bonilha et al., 2012), notably between the hippocampus and thalamus (Dinkelacker et al., 2015). There are no studies of structural connectivity in sea lions, but there is evidence of disrupted functional connectivity between the hippocampus and thalamus in wild sea lions with DA toxicosis (Cook et al., 2015), which matches findings of disrupted functional connectivity in humans with epilepsy (Waites et al., 2006; Liao et al., 2010) and rodents (Dugladze et al. 2007; Hiolski et al. 2016) and could be consistent with white matter reorganization and fornix pathology specifically.

Examination of white matter changes in wild sea lions with DA toxicosis may inform and support their potential use as a medical model. In addition, it may broaden understanding of the effects of natural exposure to DA. DA-producing algal blooms are increasingly prevalent, due in

This article is protected by copyright. All rights reserved.

Accepted Article

large part to anthropogenic influence on the oceans (Anderson et al., 2008; Silver et al., 2010). Although sea lions are the most visible victims of DA poisoning, many other species are affected, potentially including humans (Lefebvre and Robertson, 2010; Lefebvre et al., 2016). More broadly, there have been no DTI studies of structural brain connectivity in aquatic carnivores—such studies may illuminate neurobiological adaptations to these animals' unique ecology.

Here, using a novel technique for obtaining high resolution DTI data in fixed brains (Miller et al., 2012; Berns et al., 2015), we acquired 1 mm isotropic diffusion data in 8 brains collected opportunistically from wild sea lions who were euthanized due to poor medical prognosis in a rehabilitation setting: four brains with gross signs of hippocampal atrophy and four without. Fractional anisotropy (FA) and mean diffusivity (MD), potential markers of white matter pathology, were measured in the fornix, which could be clearly and reliably demarcated in these subjects, and diffusion values in the pyramidal tract were used as a control tracts to assess non-specific baseline differences in white matter diffusivity across subjects. The total number of streamlines tracking between hippocampus and thalamus was also measured. These values were compared between DA brains and brains from animals with no neurological signs as determined by veterinary diagnosis informed by clinical examination, histopathology and hippocampal morphometrics.

Materials and Methods

Subjects

This article is protected by copyright. All rights reserved.

Accepted Article

Brains for this study were obtained opportunistically from animals euthanized for medical cause at The Marine Mammal Center in Sausalito, CA. Eight brains were imaged for DTI analysis, four brains showing gross signs of hippocampal atrophy during preliminary MRI scanning, and four with no evident signs of gross neuropathology. Brains had been extracted within 24 hours of animal death, and fixed in 10% formalin for two weeks at ~4.5 degrees C before being shipped to Emory University for diffusion imaging.

Final diagnoses used to group the brains for comparison were determined post-hoc by an experienced veterinarian drawing on all available information on each animal from admission to post-mortem examination (as in Cook et al. 2015), and in keeping with best clinical practice informed by over two decades of extensive veterinary research with this population (Scholin et al. 2000; Gulland et al. 2002; Goldstein et al. 2008; Kirkley et al. 2014). Sea lions were diagnosed with carcinoma, malnutrition, and domoic acid toxicosis as described in Grieg et al. (2005). Clinical diagnosis of DA toxicosis is based on the combination of clinical signs, elevated eosinophils on CBC, ultrasound evidence of cardiomyopathy, and histology. Most DA cases display neurologic signs of seizures, ataxia, head weaving, tremoring, central blindness, blepharospasm, coma, and abnormal behavior (Gulland et al., 2002, Goldstein et al., 2008, Zabka and Gulland, 2012). Chronic cases and those with cardiomyopathy are also lethargic and malnourished. Diagnoses were supported in all cases by histopathological examination of each brain (as in Silvagni et al., 2005; Goldstein et al., 2008).

Histopathology

Following imaging, brains were sectioned to include both sides of the hippocampus, and tissue sections were routinely embedded in paraffin, processed, and stained with hematoxylin and eosin

This article is protected by copyright. All rights reserved.

Accepted Article

for histopathologic evaluation. Specific neuropathology of domoic acid exposure in sea lions has been well established in prior histological work (Silvagni et al. 2005; Goldstein et al., 2008; Lefebvre et al. 2010; Buckmaster et al. 2014). Routine hematoxylin and eosin stains were chosen in the current study to efficiently highlight established neuropathology consistent with DA toxicosis if present, and also to screen broadly for other pathologic lesions.

Imaging

All imaging and imaging analysis was conducted by an individual blind to diagnoses. For imaging, the specimens were set in 2% agarose (Phenix Research Products Low EEO Molecular Biology Grade Agarose) combined with an insoluble mixture of 2 mM gadolinium (III) oxide (Acros Organics, Fisher Scientific) (Gutman et al., 2012; Berns et al., 2015). This both holds the sample in place during scanning and provides a low-intensity background to the brain tissue for visualization as well as mitigating susceptibility artifacts at the surface of the brain.

Imaging for this study was performed on a 3 T Siemens Trio scanner with standard gradients and a 32-channel head receive coil and used a similar protocol to that detailed in Berns et al. (2015). Post-mortem tissues have shorter T1 and T2 relaxation times in comparison to live tissue, which can reduce signal quality (Miller et al., 2012). Therefore, we used a diffusion-weighted steady-state free precession (DW-SSFP) sequence optimized to increase signal to noise ratio in dead brain tissue (Miller et al., 2012). One set of DW-SSFP images, weighted along 52 directions, was acquired for each brain (FOV = 128 mm, voxel size = 1 mm isotropic, TR = 31 ms, TE = 24 ms, flip angle = 35°, bandwidth = 159 Hz/pixel, q = 255 cm^{-1}, G_{max} = 38.0 mT/m, gradient duration = 15.76 ms). Another five images were acquired for each brain with the same parameters except with q = 10 cm^{-1} applied in one direction only (these take the place of b=0 scans in conventional

This article is protected by copyright. All rights reserved.

Accepted Article

spin-echo DTI acquisitions). An accurate model of the DW-SSFP signal for post-mortem tissue must include T1 and T2 values, which we calculated for each brain using T1-weighted images (TIR sequence with TR = 1000 ms, TE = 12 ms, and TI = 30, 120, 900 ms) and T2-weighted images (TSE sequence with TR = 1000 ms, TE = 14, 29, 43 ms). High-resolution (0.6 x 0.6 x 0.5 mm) structural reference images were acquired using a "trufi" 3D balanced SSFP sequence (TR = 7.09 ms, TE = 3.55 ms, flip angle = 37°). Balanced trufi images were acquired in pairs with the RF phase incrementing 0° and 180°, and were then averaged to reduce banding artifacts (Miller et al. 2011). Total acquisition for all scan sequences was approximately 7 hours for each brain. Mean B0 and trufi structural images were computed using FSL's fslmaths. Transforms were computed between diffusion and high-resolution structural space by affine transformation of the mean B0 image to the mean trufi image with FSL's FLIRT. The resultant transformation matrix was used to compute transformations from diffusion to high-resolution structural space and vice versa, for tracking and visualization respectively. All diffusion images were processed with modified FSL tools that account for the DW-SSFP signal model and incorporate T1 and T2 measures.

Tractography

Tractography was conducted with a modified version of BEDPOSTX that incorporated the new signal model (Buxton, 1993; McNab et al., 2009; Miller et al., 2011) with 2 crossing fibres per voxel (Behrens et al., 2007). For voxel-wise estimates of diffusion parameters, we used a similarly modified version of DTIFIT.

Probabilistic tract tracings were used to define the fornix and the pyramidal tract for comparison of diffusion parameters between groups. The pyramidal tract was used for control, as it does not

This article is protected by copyright. All rights reserved.

Accepted Article

typically show extensive pathology in MTL epilepsy. The number of streamlines tracking between right and left hippocampus and bilateral thalamus was also computed using probabilistic tract tracings and compared between groups. All tracts used in quantitative analysis were computed using hand-drawn anatomical ROIs as seeds and targets in PROBTRACKX from FSL's FDT toolkit (Behrens et al., 2003; Behrens et al., 2007). For all tracings, we used the default 5000 streamlines from each voxel, a step length of 0.5 mm, distance correction, and a standard curvature threshold of 80°.

For subsequent tract definition, probabilistic tracts were thresholded by voxel using percentage of total streamlines from seed to that voxel. There is no way to determine appropriate threshold *a priori*, so we used thresholds of 5%, 10%, and 20%, computing diffusion values at each threshold with appropriate statistical correction for multiple comparisons.

ROI and Seed definition

All probabilistic tracing for this study was conducted using hand-drawn anatomical seeds, in FSL's FSLview, consistent with anatomical designations established in a prior California sea lion brain atlas (Montie et al., 2009).

Fornix tract: To accurately trace the fornix without over-representing adjacent tracts, left and right fornix were traced separately for each brain using hand-placed 12-voxel seeds in the crus of the fornix. These seeds were drawn on the FA images in DTI space, in which the forniceal white matter was easiest to visualize. Seeds were drawn with an overlaid principal diffusion map on two adjacent slices in the transverse plane. Seeds were placed in white matter with clear rostro-caudal diffusion directionality, ventral to the corpus callosum and dorsal to the dorsal boundary of the thalamus. The rostral boundary of the seeds was just caudal to the ventral turn of the

This article is protected by copyright. All rights reserved.

Accepted Article

rostral fornix, well caudal to the caudal boundary of the septum pellucidim. Medial boundaries of the seeds were lateral to midline so that they did not overlap. Two termination masks were used in tracing—a planar mask in the transverse plane at the level of the ventral boundary of the splenium and a planar mask in the coronal plane at the level of the caudal boundary of the septum pellucidum. These exclusion masks terminated any tracts that may have traveled into the corpus callosum or the septum pellucidum respectively. In all cases, probabilistic tracts from these seeds were assessed at multiple thresholds for anatomical plausibility.

Pyramidal tract: Right and left pyramidal tracts were traced for each animal using hand-placed seeds drawn on the high resolution trufi images, in which the pyramidal tract was most easily delineated from surrounding brain-stem tissue. Seeds were drawn with overlaid principle diffusion map on two consecutive slices in the coronal plane. They were placed over the full extent of the cross-section of the pyramidal tract in the brain stem, with clear rostro-caudal directionality, just caudal to the caudal boundary of the pons. Seeds were transformed into DTI space when used in BEDPOSTX. Again, probabilistic tracts from these seeds were assessed at multiple thresholds for anatomical plausibility.

Hippocampal ROI: Left and right hippocampus were traced separately by an individual with expertise in sea lion medial temporal neuroanatomy. Images were traced in the transverse plane on the high resolution trufis, in which the lateral and medial boundaries of the hippocampus were most clear (Fig. 1). Anatomical criteria were similar to those used in Cook et al. (2015). Briefly, cornu ammonis (CA), dentate gyrus, alveus, and part of the subiculum were traced in the transverse plane following the long axis of the hippocampus. Because there are no clear criteria for delineating subiculum from CA in sea lion hippocampus, tissue was taken above the interpolated line connecting the medial-most portion of parahippocampal white matter and the

John Wiley & Sons

This article is protected by copyright. All rights reserved.

Accepted Article

medial-most point on the curve of the subiculum. Hippocampus was traced from just ventral to the ventral boundary of the splenium to the rostroventral boundary of the head of the hippocampus, adjacent to the interpeduncular fossa. Lateral and medial boundaries were primarily defined by the fluid filled structures surrounding the hippocampus.

Thalamic ROI: The whole bilateral thalamus was also traced in the transverse plane, from its dorsal to ventral boundary. Thalamus was traced on B0 images in DTI space, in which thalamic boundaries with surrounding gray matter were most clearly delineated (Fig. 1).

As mentioned, all tract-based quantitative measures in the current study were computed using probabilistic tracings from FSLs BEDPOSTX. However, fornix tracts were also visualized in DSI Studio (Yeh et al., 2013), which relies on an algorithm that estimates the orientation distribution functions (ODFs) by filtering out "noisy" fibers based on a quantitative anisotropy (QA) metric, representative of diffusion strength and analogous to FA. Whole-brain and fornix renderings were computed using these parameters (unless otherwise specified): QA threshold = 0.11, angular threshold = 55°, step size = 0.50 mm, minimum length = 20 mm. 3D images of tracts were also rendered at 5° increments of rotation of the brain and assembled into movies (Mov. 1 and 2).

Quantitative Analysis

To quantify gross changes to hippocampal volume, as typically seen in sea lions with chronic DA toxicosis (Goldstein et al., 2008), volumes of right and left hippocampus were computed as percentage of whole brain volume from the same masks used as seeds for hippocampal-thalamic connectivity as in Cook et al. 2015. Standard deviation and mean relative volume of the right and left hippocampus were then computed. Animals with either right or left hippocampus volume

This article is protected by copyright. All rights reserved.

Accepted Article

more than one standard deviation below the sample mean (computed from all eight brains) were considered to have hippocampal atrophy.

Results of DTI tractography are somewhat variable based on subjectively assigned parameters, including thresholding of results (Thomas et al., 2014). However, tractography results have been repeatedly validated through both anatomical and functional connectivity approaches, and DTI is effective at capturing major fiber tracts (Catani et al., 2003; Guye et al., 2003; Wakana et al., 2004).

In the current study, fornix and pyramidal tracts were thresholded at 5%, 10%, and 20% of streamlines by voxel, then binarized. Binarized tracts at each threshold were used as masks to extract mean FA and MD values for each tract from the diffusion data maps.

For each subject, total number of streamlines tracking between right and left hippocampal seeds and bilateral thalamic endpoint was also computed. These numbers were corrected for size of hippocampal and thalamic masks so that animals with larger brain structures would not have artificially enhanced number of streamlines relative to smaller-brained subjects. Total number of streamlines for right and left hippocampus were divided by number of voxels in right and left hippocampal masks respectively, and then these values were divided by number of voxels in the bilateral thalamic masks.

Due to the small sample size in this study, standard inferential approaches may not be justified. Therefore, in addition to the qualitative observations, we used a Bayesian approach, employing Markov Chain Monte Carlo simulation (Zhao et al. 2006) to estimate the likelihood of achieving observed FA and MD values in both the control (pyramidal) and experimental (fornix) tracts between control and DA brains. Separate analyses were conducted with values from each

This article is protected by copyright. All rights reserved.

Accepted Article

streamline threshold, 5%, 10%, and 20%. We also conducted a simulation based on number of corrected streamlines between hippocampus and thalamus in healthy and DA brains. These likelihoods were then used to compute Bayes Factors, representing the likelihood ratio of two contrasting hypotheses: 1) diffusion values differ between DA and control brains, over 2) diffusion values do not differ between DA and control brains. Analysis was conducted with the anovaBF function in the BayesFactor package (Morey, Rouder & Jamil, 2015) in the R statistical software package. This function accommodates repeated measures designs (Rouder et al. 2012), taking into account the presence of a right hemisphere and left hemisphere value for each animal for each tract in the present study. For each analysis, 10,000 simulations were carried out, allowing for convergence and explicit assessment of Bayes Factors. Bayes Factors were interpreted as in Lee and Wagenmakers (2013).

Results

General Features of Sea Lion White Matter Connectivity

In examining whole-brain, deterministic maps of white matter connectivity in control sea lions (Mov. 1), a number of features stand out. Cortical projections are highly inter-digitated in all hemispheres. However, there appears to be somewhat limited rostrocaudal cortical connectivity, with a clear directional division between rostrally projecting fibers rostral to the temporal sulcus, and caudally projecting fibers caudal to the temporal sulcus, as well as very sparse cingulate fibers. In addition, sea lion corpus callosum appears thin, suggesting limited interhemispheric connectivity. Olfactory pathways also appear very small in comparison to terrestrial carnivores. The fornix appears very similar to that observed in other mammals (Fig. 2). The pyramidal tract

This article is protected by copyright. All rights reserved.

Accepted Article

is in keeping with that observed in other carnivores, with a stronger rostrocaudal gradient as compared to the dorsoventral gradient seen in primates.

Post-Hoc Diagnosis

Based on all clinical information, including histopathological analysis, three brains were determined to be from animals that had chronic DA toxicosis, and three from animals with no neurological signs or lesions (Table 1). Cases included in the DA group had hippocampal atrophy, gliosis, and neuronal loss or acute hippocampal neuronal necrosis consistent with lesions previously reported in sea lions exposed to DA (Silvangni et al., 2005). These designations were made by an experienced marine mammal veterinarian with extensive prior experience diagnosing and treating wild sea lions with DA toxicosis, in concert with an experienced veterinary histopathologist, and, given the availability of observation, brain imaging, and histopathology, they were made with a high degree of confidence. The three brains from animals with a post-hoc diagnosis of DA toxicosis had histologically identified neuronal loss and gliosis in the hippocampus (Fig. 3) and also had hippocampal atrophy per volumetry. The other three brains from sea lions without neurologic signs or lesions did not, and these three animals had received confident diagnoses of non-neurological conditions (Fig. 3). These brains were used as a DA and control group respectively, and all primary statistical comparisons were computed on these two groups. In two other cases, sea lions had evidence of cardiomyopathy often associated with DA but exhibited atypical neurological signs and/or hippocampal lesions were not completely consistent with DA toxicosis, so were analyzed separately. One brain (10840) had no histopathological signs of DA, but had age-related lesions, including axon loss with dilated axons sheaths and neuronal lipofuscinosis. This brain also exhibited hippocampal atrophy via volumetry. The other brain (10916) had lesions most severe in the amygdala with only very

This article is protected by copyright. All rights reserved.

Accepted Article

mild changes in the hippocampus. Amygdala lesions in this animal included marked gliosis, non-suppurative inflammation and mild neuronal necrosis (Figs. ~~3E~~ 3e and ~~F~~f). Mild widespread encephalitis was also identified throughout the brain. This brain exhibited no evidence of hippocampal atrophy. Neither brain, and neither animal, exhibited clear signs of chronic DA toxicosis as established in the veterinary literature.

Diffusion Measures

Probabilistic fornix tracings did not extend ventrally into the fimbria, likely due to termination of fibers traveling dorsal to the ventral boundary of the corpus callosum and due to thresholding (Fig 4). Because partial voluming effects complicate tractography in the fimbria (Concha et al., 2010), this was deemed acceptable. Although tracts did not survive into the fimbria, they were judged anatomically plausible representations of the body and pillar of the fornix for each subject. Pyramidal tracts proceeded from brainstem through rostral internal capsule (Fig. 4)

Although the cingulate was initially judged a promising target for tractography, due to its involvement in human epilepsy and relative ease of identification, cingulate fibers were extremely thin in all imaged brains, and could not be traced at reasonable diffusivity thresholds. This may be a feature of the pinniped brain, and bears further examination.

Two other tracts commonly examined in human epilepsy, the uncinate and arcuate fasciculi, have not been identified in the pinniped brain, and are defined by connection to cortical regions that have not been functionally delineated in the sea lion brain. These may also bear further examination.

Bayes Factors for comparisons of fornix FA values between control and DA brains were greater than 3 at each tract tracing threshold, indicating moderate or greater evidence for a meaningful

This article is protected by copyright. All rights reserved.

Accepted Article

difference between the two groups (5% threshold: 3.23 +/- 1.35; 10% threshold: 18.06 +/1 2.09; 20% threshold: 4.39 +/- 1.13). FA values were lower in the DA than control group (Fig.5) Bayes Factors for comparisons of fornix MD values between control and DA brains were between 1 and 2 at each tract tracing threshold, indicating slight anecdotal evidence for a meaningful difference between groups (5% threshold; 1.12 +/- 1.09; 10% threshold; 1.74 +/- 0.72; 20% threshold; 1.28 +/- 0.76) (Fig. 5). MD values were higher in the DA than the control group (Fig. 5). All Bayes Factors values for comparisons of pyramidal control tracts, for both FA and MD, were between 0.5 and 1, indicating slight anecdotal evidence for no difference between groups (5% threshold: FA, .60 +/- 1.02; MD, 0.66 +/- 0.53; 10% threshold: FA, 0.60 +/- 0.64; MD, 0.68 +/- 0.9; 20% threshold: FA, 0.82 +/- 1.82; MD, 0.80 +/- 2.16) (Fig. 5). Bayes Factor for the comparison between hippocampal-thalamic streamlines between control and DA brains was on the cusp between anecdotal and moderate evidence for a difference between groups (2.96 +/- 0.92) (Fig. 6).

CSL 10840, the brain with age-related neural signs but no evidence of DA toxicosis, had forniceal diffusion values more consistent with those of the DA animals than with the controls at all thresholds (more than 2 s.d. below the control mean and within 1 s.d. of the DA mean). CSL 10916, the brain with histopathological signs of DA in the amygdala but not the hippocampus, had forniceal diffusion values more consistent with those of the control brains than the DA brains at all thresholds tested (within 1 s.d. of the control mean, more than 2 s.d. greater than the DA mean).

This article is protected by copyright. All rights reserved.

Accepted Article

Discussion

In high-resolution post-mortem DTI, at three separate tracing thresholds, three sea lion brains with signs of chronic DA toxicosis (verified by clinical evaluation, histopathology, and hippocampal volumetrics) showed signs of reduced FA in the fornix in comparison to three brains with no neurological signs. The DA brains showed anecdotal evidence of increased MD at all three tracing thresholds. They also showed moderated signs of increased structural connectivity between the hippocampus and the thalamus. These findings are consistent with forniceal white matter pathology and increased hippocampal structural connectivity in animals with neurotoxic exposure to DA. This pattern has been observed with *in vivo* DTI assessment of human patients with MTL epilepsy (Concha et al., 2010; Otte et al., 2012; Dinkelacker et al., 2015). Together, these facts support the emerging characterization of DA toxicosis in sea lions as primarily an epileptic disease (Gulland and Ramsdell, 2014; Buckmaster et al., 2014).

Although the sample size in this study was small, including left and right diffusion values for only three DA and three control subjects, the apparent effects of DA toxicosis on white matter integrity in the fornix were notable, particularly as pertains to fractional anisotropy (FA, a measure of directional water flow in brain tissue). Apparent differences in mean diffusivity (MD, a measure of total, non-specific waterflow in brain tissue) were less clearly supported by Bayesian modeling. This may have been due to the higher variability in the MD measures than the FA and the small sample size. Alternatively, FA may be more affected in this population. Changes in FA are taken to be indicative of myelin degradation or reduction in axonal width (Cruces and Concha, 2015), while changes in MD tend to be associated with edema and necrosis. Typically, reduced FA and increased MD are seen at primary sites of neurological insult, while reduced FA with unaltered MD may be seen in secondary sites due to Wallerian degeneration

This article is protected by copyright. All rights reserved.

Accepted Article

(Werring et al., 2000) In the current study, statistical modeling showed the greatest likelihood of difference between DA and control groups for both FA and MD at the 10% threshold, which, anecdotally, was the threshold that resulted in tract tracings most resembling those published previously in other species. Imaging and histopathology of fornix and other limbic tracts in larger samples of DA-affected sea lion brains are warranted. These may confirm the striking preliminary findings we report here, but also allow for more fine-grained analyses of the range of pathology experienced by wild animals with variable exposure histories.

Importantly, human data also indicate changes in white matter in other tracts, including the cingulate, and uncinate and arcuate fasciculi. Due to sparse fibers in the sea lion cingulate and lack of functional localization required to confidently identify cortico-cortical fiber tracts in the sea lion brain, we could not examine these tracts. Future work relying on histological identification (e.g., Sawyer, Turner & Kaas, 2016) and connectivity-based parcellation of cortical regions (e.g., Beckman, Johansen-Berg & Rushworth, 2009) in the sea lion brain would be of value. Of course, not all human tracts will have analogs in the brains of other mammals. For example, the arcuate fasiculus has been examined comparatively in ape and monkey brains, with notable differences (Rilling et al, 2008).

In addition to uncertainty about changes in other cortical tracts, we were unable to fully characterize exposure history and disease course in our subjects, as details on the animal's lives prior to stranding are unknown. This is a clear limitation of natural models in comparison to standard laboratory animal models. However, sea lions with DA toxicosis have been extensively studied in clinical settings, and this allows for confident and reliable diagnosis, particularly when structural brain imaging and post-mortem histology are available. While a number of naturally occurring conditions may lead to seizures or hippocampal damage, the histopathological

This article is protected by copyright. All rights reserved.

characteristics of domoic acid exposure in sea lions have been well characterized in repeated studies (Silvagni et al. 2005; Goldstein et al. 2008). In the current study, the clinical history of each of our subjects was carefully considered before diagnosis.

While alternative and opportunistic models of epilepsy and DA toxicosis specifically, are not suited to fully replace more accessible and controlled rodent models, they may still be of great use, particularly as disease course in rodent models does not generalize particularly well to human epilepsy (Grone and Baraban, 2015). As a long-lived, large-bodied, large-brained wild mammal with a condition similar to human MTL epilepsy, sea lions with chronic DA toxicosis may represent an ecologically valid alternative model for human MTL epilepsy. As noted by Buckmaster et al. (2014), large numbers of wild sea lions are treated annually for DA toxicosis, during which time they might also receive experimental antiepileptogenic treatments. Novel therapies for sea lions affected by DA toxicosis could lead to improved outcomes and survivability in sea lions and be a model for human epilepsy treatments. Importantly, wild sea lions in the rehabilitation setting may suffer from multiple medical conditions—it is difficult to fully control for confounding variables. However, in this, a free ranging animal may better mirror the human medical population than do most laboratory models. In addition, the clear diagnostic distinction between acute exposure and the chronic resulting condition (Goldstein et al. 2008) allows for clinical selection of animals with appropriate disease characteristics, even in a rehabilitation setting.

Post-mortem DTI also shows promise for better characterizing the specific network effects of DA toxicosis and resultant chronic MTL epilepsy. Large numbers of sea lions are euthanized each year with intractable DA toxicosis, many with full veterinary workups and diagnoses, so a large number of brains may be imaged opportunistically to better understand the neurobiological

Accepted Article

This article is protected by copyright. All rights reserved.

Accepted Article

effects of the disease. This approach may be of particular use in examining the developmental effects of DA exposures. It's known that sea lion fetuses are exposed to DA *in utero* when pregnant mothers receive high enough doses of the toxin (Ramsdell and Zabka, 2008), but the long-term neural effects of this are unknown. In addition, it's been shown that DA-related hippocampal pathology worsens with age in sea lions (Montie et al., 2012). In both cases, opportunistic examinations of white matter pathology and brain connectivity may better characterize the impact of exposure across the lifespan. Such studies are limited by incomplete patient histories, but due to tagging, rehabilitation, and rerelease, a number of animals are available for repeated behavioral testing, and disease course can be partially inferred from animal's age and neuropathology.

The current findings also extend our understanding of the likely neurobehavioral effects of DA toxicosis in wild sea lions. Cruces and Concha (2015) have characterized epilepsy as primarily a brain network disease, as opposed to a limited focal brain disorder. Alterations across brain networks will have notable effects on cognitive and behavioral processes in animals afflicted with epilepsy. Prior evidence in wild sea lions with DA toxicosis showed disrupted functional connectivity between the hippocampus and the thalamus as well as spatial memory deficits (Cook et al., 2015). Our finding of altered white matter characteristics of the fornix and potentially increased structural connectivity between the hippocampus and thalamus in sea lions with DA toxicosis expand our understanding of the neurobehavioral effects of DA toxicosis. The fornix is one of the primary pathways from the hippocampus to the thalamus (Aggleton et al., 2010), and this pathway is known essential for supporting episodic and spatial memory (Aggleton, Neave, Nagle and Hunt, 1995; Aggleton and Brown, 1999). Structural damage to this pathway can lead to severe amnesic symptoms in humans and rodents, which could be highly

This article is protected by copyright. All rights reserved.

Accepted Article

maladaptive for flexible central-place foragers such as sea lions. Interestingly, reduced forniceal FA in human patients has not been previously associated with specific memory deficits; rather, it has been linked with deficits in processing speed (McDonald et al., 2008; Alexander et al., 2014), suggesting a novel line of behavioral testing with DA-exposed sea lions.

Opportunistic post-mortem DTI may be a generally useful technique for probing the effects of environmental exposures and naturally occurring neural conditions. This was highlighted in the present study by identification of two brains with neurological signs not consistent with the typical presentation of DA toxicosis. These were treated as provisional case studies. One showed histopathological signs of DA toxicosis in the amygdala, but not the hippocampus. This animal had no hippocampal atrophy and no signs of fornix pathology. DA has been shown to target the amygdala, but has not typically been seen to do so exclusive of the hippocampus (Silvagni et al., 2005). If the insult to the amygdala in this brain was DA-related, this suggests a novel disease presentation bearing further examination.

Another brain had potentially age-related brain lesions, hippocampal atrophy, and altered forniceal diffusion, but no clear signs of DA toxicosis. Pathological aging in humans has been shown to cause hippocampal atrophy and forniceal pathology (Jack et al., 2000; Rose et al., 2000; Acosta et al., 2010). Notably, age-related neuropathology can result in seizures in humans (Romanelli et al. 1990) and in mouse models of neurobiological aging (Palop et al. 2007), which could complicate attempts to differentiate insult from normal aging versus long-term effects of DA exposure. A number of other conditions may also lead to hippocampal damage and epilepsy, including conditions involving encephalitis such as anti-AMPAR (Lancaster, Martinez-Hernandez & Dalmau, 2011). None-the-less, the anecdotal finding of potential age-related neural changes in a wild sea lions is intriguing, and raises the possibility that opportunistic post-mortem

This article is protected by copyright. All rights reserved.

Accepted Article

imaging might be used to study ecologically valid models of neural aging in large-brained, long-lived mammals, not practically done in the laboratory setting in any reasonable time-frame. Importantly, it also suggests that age-related changes may interact with DA-related changes in the wild sea lion brain.

Naturally occurring exposure to DA is an increasing threat to wild animals and potentially to humans (McCabe et al. 2016; Ferriss et al. 2017). Opportunistic post-mortem DTI can help characterize the effect of this toxin in a range of otherwise inaccessible species. Findings may also further the use of natural models for epilepsy. More generally, post-mortem DTI allows neurological assessment of a great many species not typically studied, and may increase understanding of naturally occurring disease processes as well as comparative neurobiology. Given success in obtaining in vivo MRI and fMRI measures in anesthetized sea lions (Cook et al. 2015), future studies might also attempt to obtain in vivo DTI measures from animals in a rehabilitation setting. This could broaden the range of available subjects, and, in certain circumstances, allow for longitudinal assessment of specific neural tracts. Such data could meaningfully inform work conducted with post-mortem brains, and vice versa.

Acknowledgements: The authors thank Karla Miller, Sean Foxley and Saad Jbabdi of Oxford University for support in sequence implementation and data analysis. The authors further thank the veterinary pathology team at The Marine Mammal Center for support in specimen acquisition. Imaging data acquisition was supported by an internal FERN grant to P.F.C. The authors declare no competing financial interests.

This article is protected by copyright. All rights reserved.

Accepted Article

Conflict of Interest Statement: None of the authors report any conflicts of interest.

Role of Authors: All authors had full access to all the data in the study and take responsibility for the integrity of the data and the accuracy of the data analysis. Study concept and design: PC, GB, FG. Acquisition of data: PC, GB, KC, SJ. Analysis and interpretation of data: PC, SJ, KC. Drafting of the manuscript: PC. Critical revision of the manuscript for important intellectual content: PC. Statistical analysis: PC.

Literature Cited

Acosta-Cabronero J, Williams GB, Pengas G, Nestor PJ. 2010. Absolute diffusivities define the landscape of white matter degeneration in Alzheimer's disease. Brain 133(2):529-39.

Aggleton JP, Brown MW. 1999. Episodic memory, amnesia, and the hippocampal–anterior thalamic axis. Behav Brain Sci 22(03):425-44.

Aggleton JP, Neave N, Nagle S, Hunt PR. 1995. A comparison of the effects of anterior thalamic, mamillary body and fornix lesions on reinforced spatial alternation. Behav Brain Sci 68(1):91-101.

Aggleton JP, O'Mara SM, Vann SD, Wright NF, Tsanov M, Erichsen JT. 2010. Hippocampal–anterior thalamic pathways for memory: uncovering a network of direct and indirect actions. Eur J Neurosci 31(12):2292-307.

This article is protected by copyright. All rights reserved.

Accepted Article

Alexander RP, Concha L, Snyder TJ, Beaulieu C, Gross DW. 2014. Correlations between Limbic White Matter and Cognitive Function in Temporal-Lobe Epilepsy, Preliminary Findings. Front Aging Neurosci 6:142.

Anderson DM, Burkholder JM, Cochlan WP, Glibert PM, Gobler CJ, Heil CA, Kudela RM, Parsons ML, Rensel JJ, Townsend DW, Trainer VL. 2008. Harmful algal blooms and eutrophication: examining linkages from selected coastal regions of the United States. Harmful Algae 8(1):39-53.

Behrens TE, Woolrich MW, Jenkinson M, Johansen-Berg H, Nunes RG, Clare S, Matthews PM, Brady JM, Smith SM. 2003. Characterization and propagation of uncertainty in diffusion-weighted MR imaging. Magn Reson Med 50(5):1077-88.

Beckmann, M., Johansen-Berg, H., & Rushworth, M. F. 2009. Connectivity-based parcellation of human cingulate cortex and its relation to functional specialization. Journal of Neuroscience, 29(4), 1175-1190.

Behrens TE, Berg HJ, Jbabdi S, Rushworth MF, Woolrich MW. 2007. Probabilistic diffusion tractography with multiple fibre orientations: What can we gain? Neuroimage 34(1):144-55.

Bernabeu R, Sharp FR. 2000. NMDA and AMPA/kainate glutamate receptors modulate dentate neurogenesis and CA3 synapsin-I in normal and ischemic hippocampus. J Cerebr Blood F Met 20(12):1669-80.

Berns GS, Cook PF, Foxley S, Jbabdi S, Miller KL, Marino L. 2015. Diffusion tensor imaging of dolphin brains reveals direct auditory pathway to temporal lobe. Proc R Soc B 282(1811):1203.

This article is protected by copyright. All rights reserved.

Accepted Article

Bonilha L, Nesland T, Martz GU, Joseph JE, Spampinato MV, Edwards JC, Tabesh A. 2012. Medial temporal lobe epilepsy is associated with neuronal fibre loss and paradoxical increase in structural connectivity of limbic structures. J Neurol Neurosur PS jnnp-2012.

Buckmaster PS, Wen X, Toyoda I, Gulland F, Van Bonn W. 2014. Hippocampal neuropathology of domoic acid–induced epilepsy in California sea lions (Zalophus californianus). J Comp Neurol 522(7):1691-706.

Buxton RB. 1993. The diffusion sensitivity of fast steady-state free precession imaging. Magn Reson Med 29(2):235-43.

Catani M, Jones DK, Donato R. 2003. Occipito-temporal connections in the human brain. Brain 126(9):2093-107

Cook PF, Reichmuth C, Gulland F. 2011. Rapid behavioural diagnosis of domoic acid toxicosis in California sea lions. Biol Let (UK) 7(4):536-8.

Cook PF, Reichmuth C, Rouse AA, Libby LA, Dennison SE, Carmichael OT, Kruse-Elliott KT, Bloom J, Singh B, Fravel VA, Barbosa L, Stuppino JL, Van Bonn W, Gulland F, Ranganath C. 2015. Algal toxin impairs sea lion memory and hippocampal connectivity, with implications for strandings. Science 350(6267):1545-7.

Cook PF, Reichmuth C, Rouse A, Dennison S, Van Bonn B, & Gulland F. (2016). Natural exposure to domoic acid causes behavioral perseveration in Wild Sea lions: Neural underpinnings and diagnostic application. Neurotoxicology and Teratology 57: 95-105.

Concha L, Livy DJ, Beaulieu C, Wheatley BM, Gross DW. 2010. In vivo diffusion tensor imaging and histopathology of the fimbria-fornix in temporal lobe epilepsy. J Neurosci 30(3):996-1002.

This article is protected by copyright. All rights reserved.

Rodríguez-Cruces R, & Concha L. 2015. White matter in temporal lobe epilepsy: clinico-pathological correlates of water diffusion abnormalities. Quantitative imaging in medicine and surgery, 5(2), 264.

Dakshinamurti K, Sharma SK, Sundaram M. 1991. Domoic acid induced seizure activity in rats. Neurosci Lett 127(2):193-7.

Dinkelacker V, Valabregue R, Thivard L, Lehéricy S, Baulac M, Samson S, Dupont S. 2015. Hippocampal-thalamic wiring in medial temporal lobe epilepsy: Enhanced connectivity per hippocampal voxel. Epilepsia 56(8):1217-26.

Dugladze, T., Vida, I., Tort, A. B., Gross, A., Otahal, J., Heinemann, U., ... & Gloveli, T. 2007. Impaired hippocampal rhythmogenesis in a mouse model of mesial temporal lobe epilepsy. Proceedings of the National Academy of Sciences 104(44):17530-17535.

Ferriss B E, Marcinek D J, Ayres D, Borchert J, & Lefebvre KA. 2017. Acute and chronic dietary exposure to domoic acid in recreational harvesters: A survey of shellfish consumption behavior. Environment International 101:70-79.

Goldstein T, Mazet JA, Zabka TS, Langlois G, Colegrove KM, Silver M, Bargu S, Van Dolah F, Leighfield T, Conrad PA, Barakos J. 2008. Novel symptomatology and changing epidemiology of domoic acid toxicosis in California sea lions (Zalophus californianus): an increasing risk to marine mammal health. P Roy Soc B-Biol Sci 275(1632):267-76.

Govindan RM, Makki MI, Sundaram, S K, Juhász C, & Chugani HT. 2008. Diffusion tensor analysis of temporal and extra-temporal lobe tracts in temporal lobe epilepsy. Epilepsy research 80(1);30-41.

Accepted Article

This article is protected by copyright. All rights reserved.

Accepted Article

Greig DJ, Gulland F, and Kreuder C. 2005. A decade of live California sea lion (Zalophus californianus) strandings along the central California coast: causes and trends, 1991-2000. Aquatic Mammals 31(1):40-51.

Grone BP, Baraban SC. 2015. Animal models in epilepsy research: legacies and new directions. Nat Neurosci 18(3):339-43.

Gross DW. 2011. Diffusion tensor imaging in temporal lobe epilepsy. Epilepsia 52(s4):32-4.

Gulland FM, Haulena M, Fauquier D, Langlois G, Lander ME, Zabka T, Duerr R. 2002. Domoic acid toxicity in Californian sea lions (Zalophus californianus): clinical signs, treatment and survival. Vet Rec 150(15):475-80.

Gulland FMD., Hall AJ, Greig DJ, Frame ER, Colegrove KM, Booth RKN, Wasser SK, Scott-Moncrieff JCR. 2012. Evaluation of circulating eosinophil count and adrenal gland function in California sea lions naturally exposed to domoic acid. Journal of the American Veterinary Medical Association 241(7): 943-949.

Gutman DA, Keifer OP, Magnuson ME, Choi DC, Majeed W, Keilholz S, Ressler KJ. 2012. A DTI tractography analysis of infralimbic and prelimbic connectivity in the mouse using high-throughput MRI. Neuroimage 63(2):800-11.

Guye M, Parker GJ, Symms M, Boulby P, Wheeler-Kingshott CA, Salek-Haddadi A, Barker GJ, Duncan JS. 2003. Combined functional MRI and tractography to demonstrate the connectivity of the human primary motor cortex in vivo. Neuroimage 19(4):1349-60.

Hadfield JD. 2010. MCMC methods for multi-response generalized linear mixed models: the MCMCglmm R package. Journal of Statistical Software 33(2):1-22.

This article is protected by copyright. All rights reserved.

Accepted Article

Hiolski EM, Ito S, Beggs JM, Lefebvre KA, Litke AM, & Smith DR. 2016. Domoic acid disrupts the activity and connectivity of neuronal networks in organotypic brain slice cultures. Neurotoxicology 56:215-224.

Jack CR, Petersen RC, Xu Y, O'brien PC, Smith GE, Ivnik RJ, Boeve BF, Tangalos EG, Kokmen E. 2000. Rates of hippocampal atrophy correlate with change in clinical status in aging and AD. Neurology 55(4):484-90.

Jeffery B, Barlow T, Moizer K, Paul S, Boyle C. 2004. Amnesic shellfish poison. Food and Chemical Toxicology 42(4):545-57.

Kirkley KS, Madl JE, Duncan C, Gulland FM, & Tjalkens RB. 2014. Domoic acid-induced seizures in California sea lions (Zalophus californianus) are associated with neuroinflammatory brain injury. Aquatic Toxicology156:259-268.

Kola I, Landis J. 2004. Can the pharmaceutical industry reduce attrition rates? Nature Reviews Drug Discovery 3(8):711-6.

Lancaster, E., Martinez-Hernandez, E., & Dalmau, J. 2011. Encephalitis and antibodies to synaptic and neuronal cell surface proteins. Neurology 77(2):179-189.

Liao W, Zhang Z, Pan Z, Mantini D, Ding J, Duan X, Luo C, Lu G, Chen H. 2010. Altered functional connectivity and small-world in mesial temporal lobe epilepsy. PloS one 5(1):e8525.

Lee MD, & Wagenmakers EJ. 2013. Bayesian data analysis for cognitive science: A practical course.

Lefebvre KA, Robertson A, Frame ER, Colegrove KM, Nance S, Baugh KA, ... & Gulland FM. (2010). Clinical signs and histopathology associated with domoic acid poisoning in northern fur

This article is protected by copyright. All rights reserved.

seals (Callorhinus ursinus) and comparison of toxin detection methods. Harmful Algae 9(4):374-383.

Lefebvre KA, Robertson A.2010. Domoic acid and human exposure risks: a review. Toxicon 56(2):218-30.

Lefebvre KA, Quakenbush L, Frame E, Huntington KB, Sheffield G, Stimmelmayr R, Bryan A, Kendrick P, Ziel H, Goldstein T, Snyder JA. 2016. Prevalence of algal toxins in Alaskan marine mammals foraging in a changing arctic and subarctic environment. Harmful Algae 55:13-24.

Lothman EW, Collins RC. 1981. Kainic acid induced limbic seizures: metabolic, behavioral, electroencephalographic and neuropathological correlates. Brain Res 218(1):299-318.

McCabe RM, Hickey BM, Kudela RM, Lefebvre KA, Adams NG, Bill BD, ... & Trainer VL. 2016. An unprecedented coastwide toxic algal bloom linked to anomalous ocean conditions. Geophysical Research Letters 43(19).

McDonald CR, Ahmadi ME, Hagler DJ, Tecoma ES, Iragui VJ, Gharapetian L, Dale AM, Halgren E. 2008. Diffusion tensor imaging correlates of memory and language impairments in temporal lobe epilepsy. Neurology 71:1869-76.

McNab JA, Jbabdi S, Deoni SC, Douaud G, Behrens TE, Miller KL. 2009. High resolution diffusion-weighted imaging in fixed human brain using diffusion-weighted steady state free precession. Neuroimage 46(3):775-85.

Miller KL, Stagg CJ, Douaud G, Jbabdi S, Smith SM, Behrens TE, Jenkinson M, Chance SA, Esiri MM, Voets NL, Jenkinson N. 2011. Diffusion imaging of whole, post-mortem human brains on a clinical MRI scanner. Neuroimage 57(1):167-81.

Accepted Article

This article is protected by copyright. All rights reserved.

Accepted Article

Miller KL, McNab JA, Jbabdi S, Douaud G. 2012. Diffusion tractography of post-mortem human brains: optimization and comparison of spin echo and steady-state free precession techniques. Neuroimage 59(3):2284-97.

Mishra AM, Bai H, Gribizis A, Blumenfeld H. 2011. Neuroimaging biomarkers of epileptogenesis. Neuroscience Letters 497(3):194-204.

Montie EW, Pussini N, Schneider GE, Battey TW, Dennison S, Barakos J, Gulland F. 2009. Neuroanatomy and volumes of brain structures of a live California sea lion (Zalophus californianus) from magnetic resonance images. Anatomical Record 292(10):1523-47.

Montie EW, Wheeler E, Pussini N, Battey TW, Barakos J, Dennison S, Colegrove K, Gulland F. 2010. Magnetic resonance imaging quality and volumes of brain structures from live and postmortem imaging of California sea lions with clinical signs of domoic acid toxicosis. Diseases of Aquatic Organisms 91(3):243-56.

Montie EW, Wheeler E, Pussini N, Battey TW, Van Bonn W, Gulland F. 2012. Magnetic resonance imaging reveals that brain atrophy is more severe in older California sea lions with domoic acid toxicosis. Harmful Algae 20:19-29.

Morey RD, Rouder JN, & Jamil T. 2015. BayesFactor: Computation of Bayes factors for common designs. *R package version 0.9*, *9*.

Muha N, Ramsdell JS. 2011. Domoic acid induced seizures progress to a chronic state of epilepsy in rats. Toxicon 57(1):168-71.

Otte WM, van Eijsden P, Sander JW, Duncan JS, Dijkhuizen RM, Braun KP. 2012. A meta-analysis of white matter changes in temporal lobe epilepsy as studied with diffusion tensor imaging. Epilepsia 53(4):659-67.

This article is protected by copyright. All rights reserved.

Accepted Article

Palop, J J, Chin J, Roberson ED, Wang J, Thwin, MT, Bien-Ly N, ... & Finkbeiner S. 2007. Aberrant excitatory neuronal activity and compensatory remodeling of inhibitory hippocampal circuits in mouse models of Alzheimer's disease. Neuron 55(5):697-711.

Perl TM, Bédard L, Kosatsky T, Hockin JC, Todd EC, Remis RS. 1990. An outbreak of toxic encephalopathy caused by eating mussels contaminated with domoic acid. New England Journal of Medicine 322(25):1775-80.

Pierpaoli C, Barnett A, Pajevic S, et al. 2001. Water diffusion changes in Wallerian degeneration and their dependence on white matter architecture. Neuroimage 13:1174–1185.

Pulido OM. 2008. Domoic acid toxicologic pathology: a review. Marine Drugs 6(2):180-219.

Ramsdell JS, Zabka T. 2008. In utero domoic acid toxicity: a fetal basis to adult disease in the California sea lion (Zalophus californianus). Marine Drugs 6(2):262-90.

Ramsdell JS, Gulland FM. 2014. Domoic acid epileptic disease. Marine Drugs 12(3):1185-207.

Rose SE, Chen F, Chalk JB, Zelaya FO, Strugnell WE, Benson M, Semple J, Doddrell DM. 2000. Loss of connectivity in Alzheimer's disease: an evaluation of white matter tract integrity with colour coded MR diffusion tensor imaging. Journal of Neurology, Neurosurgery & Psychiatry 69(4):528-30.

Rilling, JK, Glasser MF, Preuss TM, Ma X, Zhao T, Hu X, & Behrens TE. 2008. The evolution of the arcuate fasciculus revealed with comparative DTI. Nature Neuroscience 11(4):426.

Romanelli MF, Morris JC, Ashkin K, & Coben LA. 1990. Advanced Alzheimer's disease is a risk factor for late-onset seizures. Archives of Neurology 47(8):847-850.

Rouder, JN, Morey, RD, Speckman PL, Province JM, 2012. Default Bayes Factors for ANOVA Designs. Journal of Mathematical Psychology 56:356-374.

This article is protected by copyright. All rights reserved.

Sawyer EK, Turner EC, & Kaas J H 2016. Somatosensory brainstem, thalamus, and cortex of the California sea lion (Zalophus californianus). Journal of Comparative Neurology 524(9):1957-1975.

Scholin CA, Gulland F, Doucette GJ, Benson S, Busman M, Chavez FP, Cordaro J, DeLong R, De Vogelaere A, Harvey J, Haulena M. 2000. Mortality of sea lions along the central California coast linked to a toxic diatom bloom. Nature, 403(6765), 80-4.

Silvagni PA, Lowenstine LJ, Spraker T, Lipscomb TP, Gulland FM. 2005. Pathology of domoic acid toxicity in California sea lions (Zalophus californianus). Veterinary Pathology 42(2):184-91.

Silver MW, Bargu S, Coale SL, Benitez-Nelson CR, Garcia AC, Roberts KJ, Sekula-Wood E, Bruland KW, Coale KH. 2010. Toxic diatoms and domoic acid in natural and iron enriched waters of the oceanic Pacific. Proceedings of the National Academy of Sciences USA 107(48):20762-7.

Thomas K, Harvey JT, Goldstein T, Barakos J, Gulland F. 2010. Movement, dive behavior, and survival of California sea lions (Zalophus californianus) posttreatment for domoic acid toxicosis. Marine Mammal Science 26(1):36-52.

Thomas C, Frank QY, Irfanoglu MO, Modi P, Saleem KS, Leopold DA, Pierpaoli C. 2014. Anatomical accuracy of brain connections derived from diffusion MRI tractography is inherently limited. Proceedings of the National Academy of Sciences USA 111(46):16574-9.

Yeh FC, Verstynen TD, Wang Y, Fernández-Miranda JC, Tseng WY. 2013. Deterministic diffusion fiber tracking improved by quantitative anisotropy. PloS one 8(11):e80713.

Wakana S, Jiang H, Nagae-Poetscher LM, Van Zijl PC, Mori S. 2004. Fiber tract–based atlas of human white matter anatomy 1. Radiology 230(1):77-87.

Accepted Article

This article is protected by copyright. All rights reserved.

Accepted Article

Waites AB, Briellmann RS, Saling MM, Abbott DF, Jackson GD. 2006. Functional connectivity networks are disrupted in left temporal lobe epilepsy. Annals of Neurology 59(2):335-43.

Werring DJ, Toosy AT, Clark CA, et al. 2000. Diffusion tensor imaging can detect and quantify corticospinal tract degeneration after stroke. J Neurol Neurosurg Psychiatry, 69:269–272.

Zabka TS, Goldstein T, Cross C, Mueller RW, Kreuder-Johnson C, Gill S, Gulland FMD. 2009. Characterization of a degenerative cardiomyopathy associated with domoic acid toxicity in California sea lions (Zalophus californianus). Veterinary Pathology 46: 105-119.

Zhao Y, Staudenmayer J, Coull BA, Wand MP.2006. "General design Bayesian generalized linear mixed models." Statistical Science 21(1):35–51.

Figure 1: Hippocampal and Thalamic Regions of Interest. Representative ROIs from one control subject, 10814. ROIs were drawn using FSL's FSLView in the transverse plane. Hippocampal ROIs were drawn directly on trufi images. Thalamic ROIs were drawn on B0 images and transformed to trufi space for visualization. ~~A~~a) Three representative hippocampal tracings from along the longitudinal axis of the hippocampus, shown at left. The red transects show tracings on a dorsocaudal slice, just ventral to the splenium (top), a slice from the middle of the hippocampus adjacent and lateral to the inferior colliculi (middle), and a ventrorostral slice, adjacent and lateral to the interpeduncular fossa (bottom). Left hippocampal regions are shown in red (on the right side of the image in radiological presentation), and right regions are left bare for visualization. ~~B~~b) Right thalamus is shown (on the left side of each image) in three

Comment [PC1]: Fig 2(?) in results, right before deterministic fig…

This article is protected by copyright. All rights reserved.

Accepted Article

imaging planes, transverse (left), sagittal (middle), and coronal (right). Thalamus was traced bilaterally in one mask, but left thalamus is uncovered here for purposes of visualization.

Figure 2: Deterministic Tract Renderings of Whole Brain and Fornix. Representative tract renderings from one control subject, 10814, produced in DSI studio. ~~A~~a) Whole brain rendering of sea lion white matter tracts. Viewed in the transverse plane, ventral to the brain, with rostral portion at the top of the image. Tract color represents fiber direction: green=rostral-caudal, red=left-right, blue=dorsal-ventral. The fornix is clearly visible as an inverted green "v", just caudal to the genu of the corpus callosum (large left-right red fiber bundle). The blue tip of the "v" is where the fornix takes its ventral turn into the pillar. The pyramidal tract is also visible, exiting the brain stem dorsal to the pons before heading rostrolaterally through the internal capsule to motor cortex (which is notably more rostral in the carnivore than primate brain). ~~B~~b) A fornix tracing including fimbria. This tracing was produced with a spherical seed centered on the crus of the fornix, in the same location as used to seed probabilistic tracings in FSL. Planar termination masks were placed caudal to the septum pellucidum, just ventral to the splenium, and lateral to the hippocampus. QA threshold had to be lowered (0.07) to trace into fimbria.

Comment [PC2]: Make fig 1 in methods(?)

Figure 3: Hematoxylin and eosin stained sections of brain from sea lions illustrating histological lesions characteristic of typical and atypical DA toxicosis. a) Hippocampus from a normal California sea lion (case 11141). DG = Dentate gyrus; CA = cornu ammonis. Bar = 500 µm. b) Higher power image of the hippocampus from case 11141. Note the normal hippocampal neurons (arrows). Bar = 50 µm. c). Hippocampus from a sea lion with domoic acid toxicosis (case 11217). Note the hippocampal atrophy, loss of neurons

John Wiley & Sons

This article is protected by copyright. All rights reserved.

Accepted Article

in the dentate gyrus (DG) and cornu ammonis (CA), and the increased numbers of glial cells. Bar = 500 µm. d) Higher power image of the dentate gyrus from case 11217. Note the hypereosinophilic necrotic neurons (arrows) and gliosis. Bar = 20 µm. e) Photomicrograph of the amygdala from case 10916. There is severe gliosis and inflammation. Box denotes area of high power image (f). Bar = 200 µm. f) Higher power image of the amygdala from case 10916 illustrating gliosis and perivascular chuffing with lymphocytes. Bar = 20 µm. g) Normal amygdala from case 10840. Box denotes area of high power image (h). Bar = 200 µm. h) High power image of normal amygdala. Note the small amount of light yellow lipofuscin within neurons associated with older age. Bar = 50 µm.~~**Hematoxylin and eosin stained sections of brain from sea lions illustrating histological lesions characteristic of typical and atypical DA toxicosis.** A) Hippocampus from a normal California sea lion (case 11141). DG = Dentate gyrus; CA = cornu ammonis. Bar = 500 µm. B) Higher power image of the hippocampus from case 11141. Note the normal hippocampal neurons (arrows). Bar = 50 µm. C). Hippocampus from a sea lion with domoic acid toxicosis (case 11217). Note the hippocampal atrophy, marked loss of neurons in the dentate gyrus (DG) and cornu ammonis (CA), and the increased numbers of glial cells. Bar = 500 µm. . D) Higher power image of the dentate gyrus from case 11217. Note the hypereosinophilic necrotic neurons (arrows) and gliosis. Bar = 50 µm. E) Photomicrograph of the amygdala from case 10916. There is severe gliosis and inflammation. Bar = 200 µm. F) Higher power image of the amygdala from case 10916 illustrating gliosis and perivascular chuffing with lymphocytes. Bar = 20 µm.~~

Figure 4: Probabilistic Fornix and Pyramidal Tract Tracings. Representative tracings from one control subject, 10814. Tracts were computed in diffusion space, then transformed for visual

This article is protected by copyright. All rights reserved.

presentation in high-resolution trufi space. ~~A~~a) Right (red) and left (blue) fornix tracings in the transverse, sagittal, and coronal plane, from left to right. ~~B~~b) Right (red) and left (blue) pyramidal tract tracings in the transverse, sagittal, and coronal plane from left to right. In both ~~A~~ a and ~~B~~b, right and left tracts were traced independently from separate seeds. Tracings are thresholded at 10% of streamlines, i.e., only voxels receiving 10% or more of the streamlines traced from the seed are shown.

Figure 5: ~~Decreased~~ Lower Directional Diffusion in the Fornix of a DA Brain. Fornix was traced in DSI studio using the same seed as discussed in the caption of Figure 3, but with a higher qa threshold (0.10). Color represents qa value (analogous to FA), as demonstrated in color scale bars, with warmer colors representing higher qa/greater directional water diffusion. ~~A~~a) Representative right fornix render in a control animal, 10814, shown in a sagittal slice over the FA map (left) and in a head-on coronal view extracted (right). Higher directional diffusion can be seen in the crus of the fornix represented by bright yellow. ~~B~~b) Representative right fornix render in a DA animal, 11182, with clearly ~~reduced~~ lower directional diffusion over the crus represented by deeper red. ~~C~~c) Mean FA (left column) and MD (right column) are shown on the y axis in the pyramidal (top row) and fornix (bottom row) tracts for each control and DA subject. Right and left values for each animal are shown separately. Pairs of values (right and left) for each animal are coded in the figure by shape. FA and MD values were extracted from binarized masks at the 10% by-voxel threshold. MD values have been multiplied by 1000 for presentation purposes. Plots show mean, 25th and 75th percentile within each box, with whiskers extending to the highest and lowest values within 1.5 * the inter-quartile range. Pyramidal diffusion measures were not distinct between DA and control brains. Forniceal FA was decreased and MD increased

Accepted Article

This article is protected by copyright. All rights reserved.

Accepted Article

in DA brains, indicative of white-matter pathology. ~~D~~d) Side views of right and left fornix for each subject, as computed in FSL. These are thresholded at 10% by-voxel, and represent the FA values in the 10% by-voxel thresholds masked regions. Here, color represents FA value, with higher values (greater directionality) represented as yellow.

Figure 6: ~~Increased~~ Higher Hippocampal-Thalamic Structural Connectivity in DA Brains. Number of total streamlines between right and left hippocampus and bilateral thalamus, corrected by size of hippocampal and thalamic masks, are shown for each control and DA animal. Right and left values for each animal are combined within the same box, although statistics were computed by repeated-measures ANOVA. Pairs of values (right and left) for each animal are coded in the figure by shape. Plots show mean, 25th and 75th percentile within each box, with whiskers extending to the highest and lowest values within 1.5 * the inter-quartile range.

Movie 1: Rotation of Whole Brain Deterministic Rendering of White Matter Pathways in a Control Sea Lion. Major white matter pathways at a qa threshold of 0.10. Green fibers are rostrocaudal, red are left-right, and blue are dorsoventral.

Movie 2: Rotation of Deterministic Corpus Callosum Render. Right corpus callosum of one control subject, 10814, traced as described in caption to Figure 3, shown here in green, was overlaid with a whole-brain render of white matter tracts (dark purple) and rotated for the purpose of visualization.

This article is protected by copyright. All rights reserved.

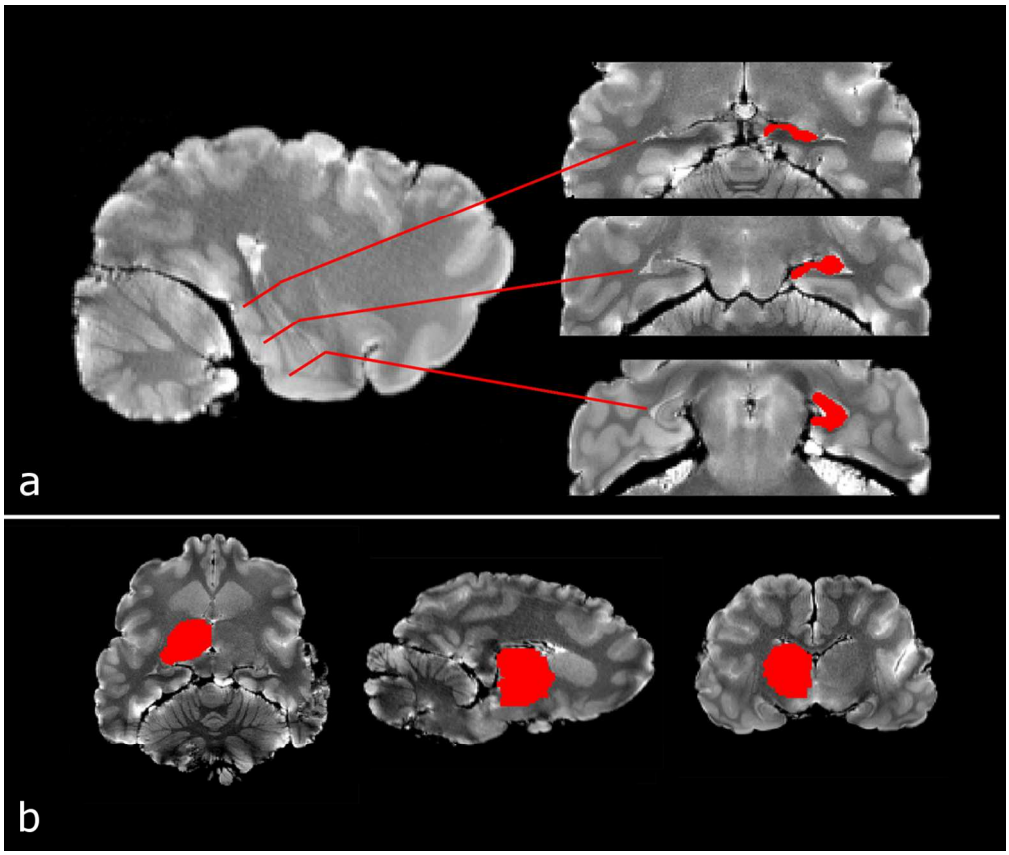

Figure 1: Hippocampal and Thalamic Regions of Interest. Representative ROIs from one control subject, 10814. ROIs were drawn using FSL's FSLView in the transverse plane. Hippocampal ROIs were drawn directly on trufi images. Thalamic ROIs were drawn on B0 images and transformed to trufi space for visualization. a) Three representative hippocampal tracings from along the longitudinal axis of the hippocampus, shown at left. The red transects show tracings on a dorsocaudal slice, just ventral to the splenium (top), a slice from the middle of the hippocampus adjacent and lateral to the inferior colliculi (middle), and a ventrorostral slice, adjacent and lateral to the interpeduncular fossa (bottom). Left hippocampal regions are shown in red (on the right side of the image in radiological presentation), and right regions are left bare for visualization. b) Right thalamus is shown (on the left side of each image) in three imaging planes, transverse (left), sagittal (middle), and coronal (right). Thalamus was traced bilaterally in one mask, but left thalamus is uncovered here for purposes of visualization.

129x109mm (300 x 300 DPI)

This article is protected by copyright. All rights reserved.

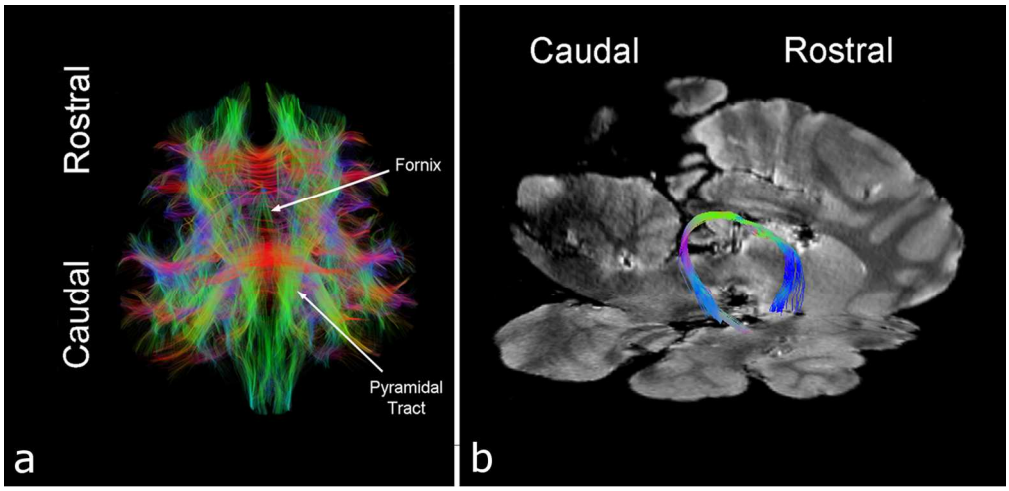

Figure 2: Deterministic Tract Renderings of Whole Brain and Fornix. Representative tract renderings from one control subject, 10814, produced in DSI studio. a) Whole brain rendering of sea lion white matter tracts. Viewed in the transverse plane, ventral to the brain, with rostral portion at the top of the image. Tract color represents fiber direction: green=rostral-caudal, red=left-right, blue=dorsal-ventral. The fornix is clearly visible as an inverted green "v", just caudal to the genu of the corpus callosum (large left-right red fiber bundle). The blue tip of the "v" is where the fornix takes its ventral turn into the pillar. The pyramidal tract is also visible, exiting the brain stem dorsal to the pons before heading rostrolaterally through the internal capsule to motor cortex (which is notably more rostral in the carnivore than primate brain). b) A fornix tracing including fimbria. This tracing was produced with a spherical seed centered on the crus of the fornix, in the same location as used to seed probabilistic tracings in FSL. Planar termination masks were placed caudal to the septum pellucidum, just ventral to the splenium, and lateral to the hippocampus. QA threshold had to be lowered (0.07) to trace into fimbria.

129x62mm (300 x 300 DPI)

Accepted

This article is protected by copyright. All rights reserved.

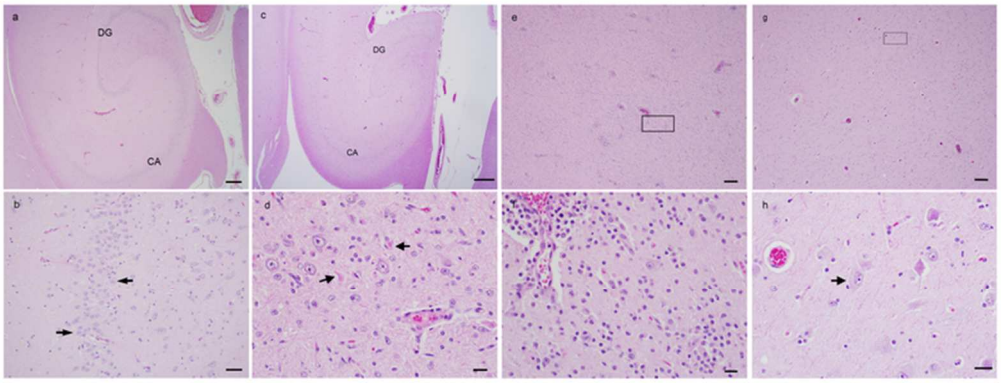

Figure 3: Hematoxylin and eosin stained sections of brain from sea lions illustrating histological lesions characteristic of typical and atypical DA toxicosis. a) Hippocampus from a normal California sea lion (case 11141). DG = Dentate gyrus; CA = cornu ammonis. Bar = 500 µm. b) Higher power image of the hippocampus from case 11141. Note the normal hippocampal neurons (arrows). Bar = 50 µm. c) Hippocampus from a sea lion with domoic acid toxicosis (case 11217). Note the hippocampal atrophy, loss of neurons in the dentate gyrus (DG) and cornu ammonis (CA), and the increased numbers of glial cells. Bar = 500 µm. d) Higher power image of the dentate gyrus from case 11217. Note the hypereosinophilic necrotic neurons (arrows) and gliosis. Bar = 20 µm. e) Photomicrograph of the amygdala from case 10916. There is severe gliosis and inflammation. Box denotes area of high power image (f). Bar = 200 µm. f) Higher power image of the amygdala from case 10916 illustrating gliosis and perivascular chuffing with lymphocytes. Bar = 20 µm. g) Normal amygdala from case 10840. Box denotes area of high power image (h). Bar = 200 µm. h) High power image of normal amygdala. Note the small amount of light yellow lipofuscin within neurons associated with older age. Bar = 50 µm.

67x26mm (300 x 300 DPI)

Accept

This article is protected by copyright. All rights reserved.

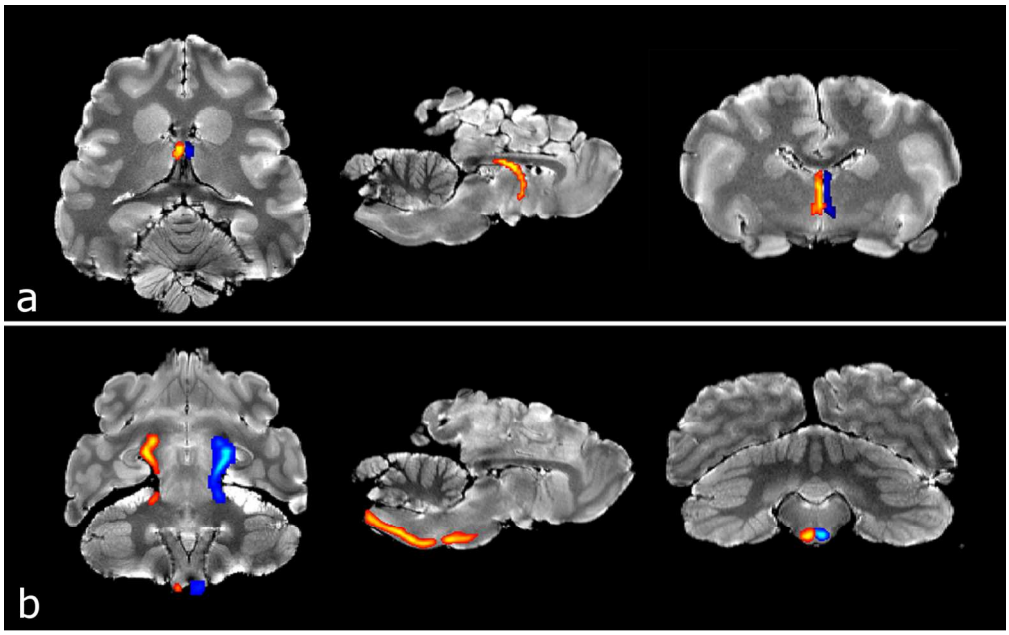

Figure 4: Probabilistic Fornix and Pyramidal Tract Tracings. Representative tracings from one control subject, 10814. Tracts were computed in diffusion space, then transformed for visual presentation in high-resolution trufi space. a) Right (red) and left (blue) fornix tracings in the transverse, sagittal, and coronal plane, from left to right. b) Right (red) and left (blue) pyramidal tract tracings in the transverse, sagittal, and coronal plane from left to right. In both a and b, right and left tracts were traced independently from separate seeds. Tracings are thresholded at 10% of streamlines, i.e., only voxels receiving 10% or more of the streamlines traced from the seed are shown.

129x81mm (300 x 300 DPI)

This article is protected by copyright. All rights reserved.

Article

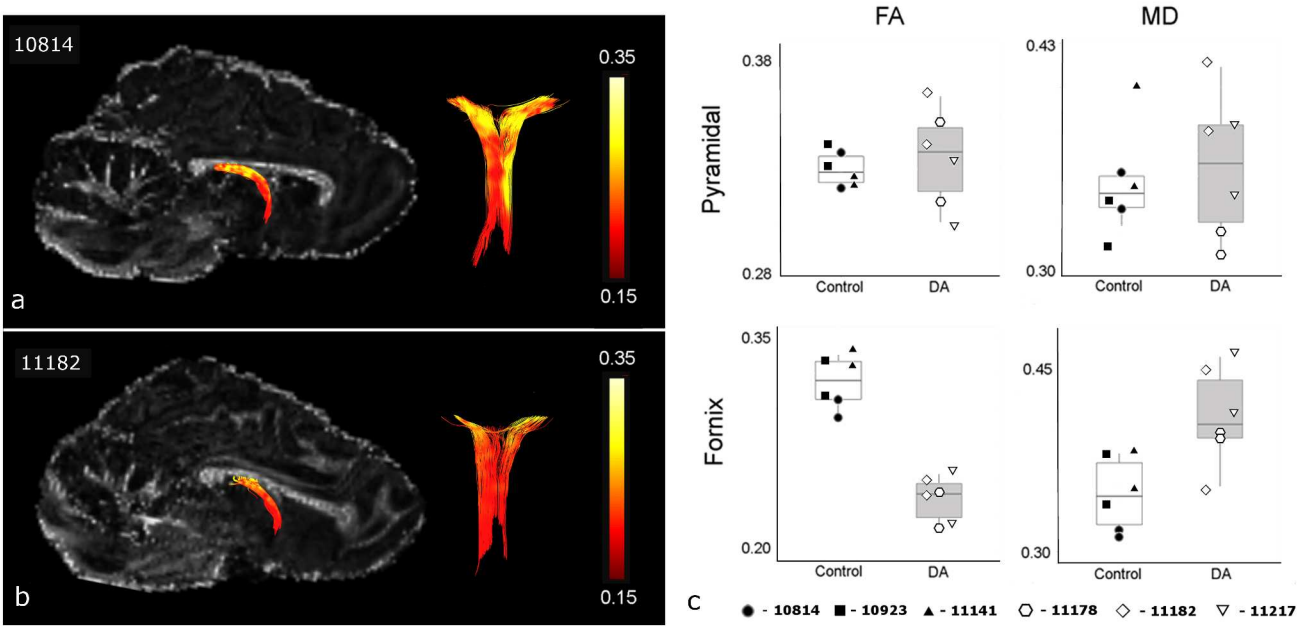

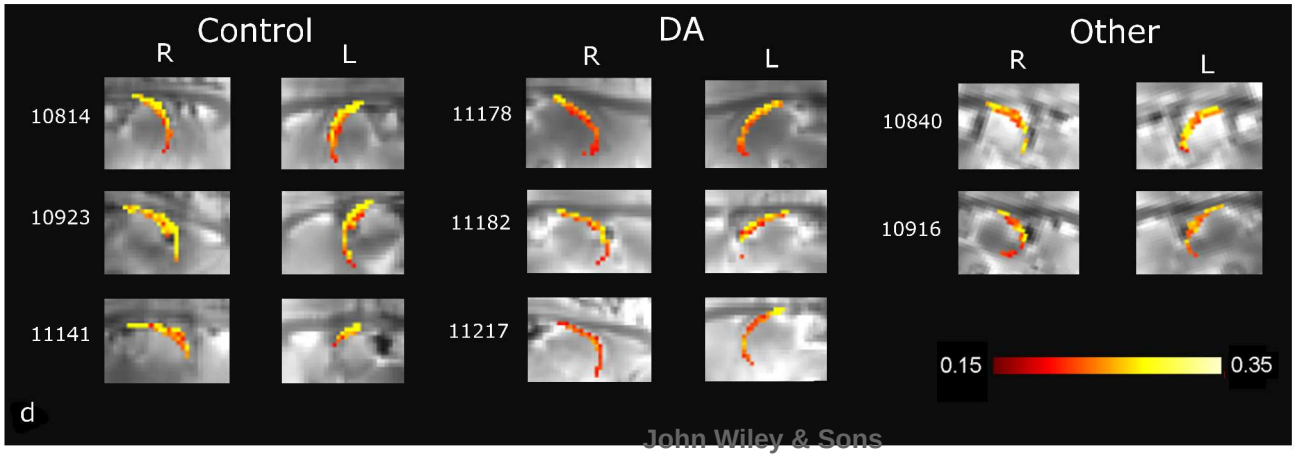

John Wiley & Sons

This article is protected by copyright. All rights reserved.

Accepted Article

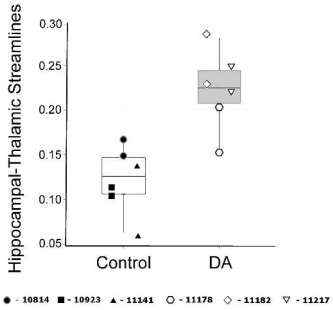

This article is protected by copyright. All rights reserved.

Subject ID	Age	Sex	Diagnosis	Histopathology	RHP Volume	LHP Volume
10814	Adult	F	Renal disease, declining condition – euthanized due to poor prognosis, metastatic carcinoma diagnosed post-mortem	Normal	0.57	0.61
10923	Pup	M	Severe emaciation and hypoglycemia resulting from malnutrition – Unresponsive to treatment, euthanasia elected due to poor prognosis	Normal	0.58	0.63
11141	Adult	F	Emaciated, severe trauma and paresis led to euthanasia - Metastatic urogenital carcinoma diagnosed post-mortem	Normal	0.57	0.52
11178	Adult	F	DA – Pneumonia, tremors and grand mal seizures – Euthanized due to poor progosis	Hippocampus – gliosis, neuronal loss	0.46	0.35
11182	Adult	F	DA – Repeated seizures despite phenobarbital treatment, eosinophilia – euthanasia elected due to no treatment response and poor prognosis	Hippocampus – gliosis, neuronal loss	0.43	0.39
11217	Juvenile	M	DA – Grade II heart murmur, eosinophilia – Euthanized due to poor prognosis	Hippocampus – gliosis, neuronal loss	0.42	0.40
10840	Adult	F	Heart disease – severe cardiomyopathy – euthanized due to severe heart disease/poor prognosis	Dilated axon sheaths	0.51	0.39
10916	Adult	F	Atypical DA - Pneumonia, unusual behavior, cardiomyopathy - Euthanized due to heart disease/poor prognosis, atypical DA	Amygdala – gliosis, neuronal necrosis	0.67	0.66

Table 1: Study Subjects Diagnostic Information. Field identification number; age as determined by veterinary assessment (pup: < 1 year old, juvenile: between 1 and 5 years old; adult: > 5 years old); final, post-hoc diagnosis and reason for euthanasia; histopathological assessment; and right (RHP) and left (LHP) hippocampal volume as a percent of whole brain volume.

This article is protected by copyright. All rights reserved.

Table 2

	Fractional Anisotropy in Fornix						Mean Diffusivity in Fornix						HP-Thalamic Streamlines	
ID	**R5**	**L5**	**R10**	**L10**	**R20**	**L20**	**R5**	**L5**	**R10**	**L10**	**R20**	**L20**	**RHP**	**LHP**
10814	0.27	0.27	0.31	0.29	0.36	0.34	0.32	0.34	0.31	0.32	0.24	0.33	0.17	0.15
10923	0.29	0.29	0.31	0.33	0.37	0.37	0.39	0.35	0.38	0.34	0.33	0.30	0.11	0.10
11141	0.36	0.29	0.34	0.33	0.25	0.39	0.40	0.38	0.38	0.35	0.39	0.34	0.14	0.06
11178	0.22	0.23	0.22	0.24	0.19	0.25	0.39	0.39	0.40	0.39	0.40	0.39	0.15	0.20
11182	0.23	0.23	0.25	0.24	0.25	0.22	0.35	0.45	0.35	0.45	0.30	0.46	0.23	0.28
11217	0.23	0.25	0.22	0.26	0.24	0.25	0.44	0.41	0.46	0.43	0.45	0.47	0.25	0.22
10840	0.28	0.27	0.29	0.29	0.27	0.36	0.33	0.38	0.34	0.37	0.27	0.25	0.18	0.15
10916	0.22	0.24	0.24	0.23	0.22	0.24	0.38	0.38	0.36	0.41	0.34	0.43	0.19	0.24

Table 2: Forniceal Diffusion Values and Hippocampal-Thalamic Streamlines. *Field Identification number, mean FA and MD values in right (R) and left (L) fornix traced at three by-voxel thresholds (5%, 10%, and 20%), and total streamlines between right (RHP) and left (LHP) hippocampus and bilateral thalamus corrected by size of hippocampal and thalamic ROIs. MD values were multipled by 1000. Controls are in white, DA animals in light gray, and the two animals with atypical neural findings in dark gray.*

Accepted Article

This article is protected by copyright. All rights reserved.

Accepted Article

Title: Post-Mortem DTI Reveals Altered Hippocampal Connectivity in Wild Sea Lions Diagnosed with Chronic Toxicosis from Algal Exposure

Authors: Peter F. Cook*, Gregory S. Berns, Kathleen Colegrove, Shawn Johnson, Frances Gulland

Summary: Wild California sea lions are frequently exposed to the algal toxin domoic acid, leading to neurological signs, seizures, and hippocampal atrophy. Using opportunistic post-mortem diffusion tensor imaging of wild sea lion brains, we show altered diffusion properties in the fornix of animals with a likely history of exposure to domoic acid. These findings extend knowledge of the neurobiological effects of this common natural toxin, and match those observed in humans with medial temporal epilepsy.

This article is protected by copyright. All rights reserved.

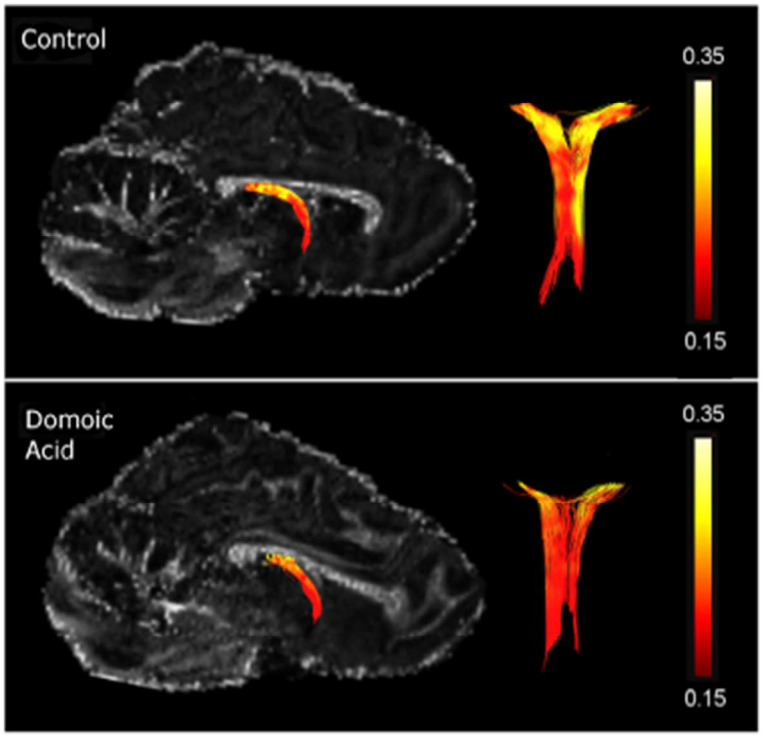

141x141mm (72 x 72 DPI)

Accep

This article is protected by copyright. All rights reserved.